In the Case of Maden Complex, Geochemical Constraints on the Origin and Tectonic Implication of Eocene Magmatism in SE Turkey

Mehmet ali Ertürk*[,1], Melahat Beyarslan[1], Abdullah Sar[1]

1- Department of Geological Engineering, Fırat University, 23119 Elazığ/Turkey.

* Corresponding Author: erturkmae@gmail.com

Received: 06 April, 2018 / Accepted: 03 June 2018 / Published online: 06 June 2018

Abstract

The origin and geodynamic setting of the Maden Complex, which is situated in the Bitlis–Zagros Suture Zone in the Southeast Anatolian Orogenic Belt, is still controversial due to lack of systematic geological and geochemical data. Here we present new whole rock major–trace–rare earth element data from the Middle Eocene volcanic rocks exposed in Maden Complex and discuss their origin in the light of new and old data. The volcanic lithologies are represented mainly by basalt and andesite, and subordinately dacite that vary from low–K tholeiitic, calc–alkaline, high–K calc–alkaline, and shoshonitic in composition. They exhibit enrichments in large ion lithophile and light rare earth elements, with depletions in high field strength elements. These geochemical characteristics indicate that two end–members, a subduction–related mantle source and a continental crust, were involved in the magma genesis. Considering all geological and geochemical data, we suggest that the Middle Eocene Maden magmatism occurred as a post–collisional product by asthenospheric upwelling owing to convective removal of the lithosphere during an extensional collapse of the Southeast Anatolian ranges.

Keywords: Middle Eocene; Maden Complex; Southeast Anatolian Orogenic Belt; Asthenospheric Upwelling.

1- Introduction

The Southeast Anatolian Orogenic Belt (SAOB) constitutes the eastern part of the Taurus Orogenic Belt, which is one of the most important tectonic belts in Turkey, located between the Anatolid/Tauride Platform and the Arabian Plate. This belt is a very complex segment of the Alpine–Himalayan mountain chain and has many specific features. Magmatism from the Ediacaran period up to the Quaternary has occurred in different geodynamic environments. The most intense periods of magmatism were the Ediacaran, Late Triassic to Late Cretaceous, Middle Eocene and Late Miocene (Şengör and Yılmaz, 1981; Yazgan, 1983; Bingöl, 1994; Yılmaz, 1993; Keskin, 2003, 2007; Şengör *et al*., 2008; Ustaömer *et al*., 2009; Gürsu *et al*., 2015; Beyarslan *et al*., 2016). From a tectonic point of view, orogenic magmatism refers to igneous activity associated with subduction of oceanic lithosphere or continent–continent collision (e.g. the Anatolide and Arabian Plate; Lustrino and Wilson, 2007).

The study area is located on the Bitlis–Zagros suture zone (Fig 1). The Maden complex is most commonly found in two regions; the Maden–Ergani region (south of Elazığ) and the Pütürge–Kale region (southeast of Malatya). In both regions, the Arabian Plate and accretionary complex are exposed. In these areas where the Maden Complex crops out, Neoproterozoic–

Early Cambrian Pütürge metamorphics (Ustaömer *et al*., 2009, 2012; Beyarslan *et al*., 2016), Late Cretaceous ophiolitic massifs and Late Cretaceous intra–oceanic arc–type magmatics (Elazığ magmatics) belonging to the nappe zone are exposed (Yazgan, 1984; Yazgan and Chessex, 1991; Parlak *et al*., 2009; Robertson *et al*., 2012; Karaoğlan *et al*., 2012; 2013a, b, c; 2016; Beyarslan and Bingöl, 2014; Bingöl *et al*., 2014; Lin *et al*., 2015; Tekin *et al*., 2015; Ural *et al*., 2015; Rizeli *et al*., 2016).

Petrographical studies and geochemical analyses (major element–trace element–rare earth element concentrations) were conducted to determine the origin and geological setting of rocks within the Maden Complex. Based on the obtained petrogenetic results and field observations, it was interpreted the evolution of the region in the Eocene period.

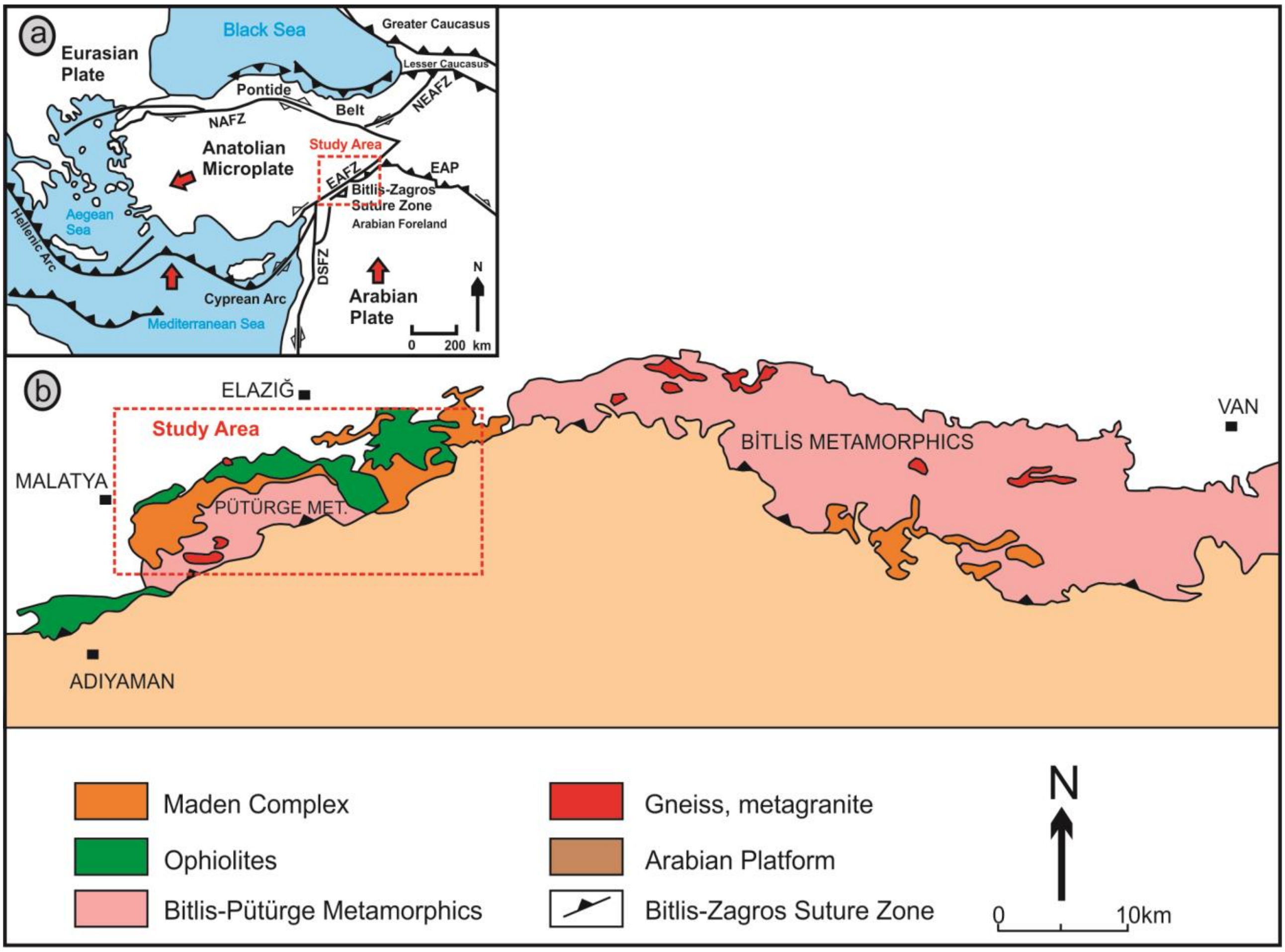

Figure 1a) The modern or neotectonic setting of eastern Turkey (Nicoll, 2010), NAFZ = North Anatolian Fault Zone, NEAFZ = Northeast Anatolian Fault zone, EAFZ = East Anatolian Fault Zone, EAP = Eastern Anatolian Plateau, (b) The distribution of the Eocene Magmatic Rocks in the Southeast Anatolia (Turkey) (simplified from MTA, 2002).

2- Geological setting

The SAOB has been divided into three major tectonic zones by (Yılmaz, 1993): namely (1) Arabian Plate (2) "Zone of Imbrication", which occurs in the north of the Arabian Plate, forming a reverse fault zone developed in the Late Cretaceous–Early Miocene interval, approximately 5–10 km in width, (3) "Nappe Zone". The three zones are separated from each other by thrust faults (Yılmaz, 1993; Yılmaz *et al*., 1993).

2.1- The Arabian Plate

The Arabian Plate is represented by a range of units, from Pre–Cambrian non–metamorphic volcanics to the Early Miocene Lice Formation (Yılmaz, 1993; Gürsu *et al*., 2015). In southeastern Turkey, Ediacaran–Earliest Cambrian units are best exposed in the Zap Valley and in the Derik (Mardin) area. Derik (Mardin) area is located along the northernmost margin of the Arabian Plate. The basal section of the Derik area consists of non–metamorphosed volcanic rocks, conglomerates and fine/coarse sandstones (Göncüoğlu and Kozlu, 2000; Ghienne *et al*., 2010). The area includes Cambrian to Early Carboniferous clastics and limestones unconformably overlying Triassic to Cretaceous platform–type carbonates, and Maastrichtian to Early Miocene clastics and carbonates (Perinçek, 1978; Yılmaz, 1993; Ghienne *et al*., 2010; Beyarslan *et al*., 2016; Robertson *et al*., 2016). The uppermost part of the Arabian Plate is represented by the Early Miocene Lice Formation.

The imbricated zone represents the Bitlis–Zagros Suture Zone between the Arabian Plate and the Nappe Zone. This suture zone is marked by ophiolites that formed in a supra–subduction zone (Şengör and Yılmaz, 1981; Yazgan and Chessex, 1991; Yılmaz, 1993; Robertson *et al*., 2004, 2007; Parlak *et al*., 2009; Beyarslan and Bingöl, 2010, 2014).

2.2- Late Cretaceous Koçali complex

The Koçali Complex was initially named the Koçali unit by Sungurlu (1974) at the north of Adıyaman. The Complex was later subdivided into the Tarasa, Konak, and Kale formations by Perinçek (1978, 1979). According to Beyarslan (2017), the Tarasa formation is composed of basaltic volcanic rocks; the Konak formation consists of limestones, radiolarites, and volcanics; and the Kale formation constitutes the upper part of the Koçali Complex and is comprised of mantle peridotites, gabbros, diabase, and basic volcanic rocks. Bingöl (1994) named this formation as the Koçali Ophiolite in the Çermik area (northwest of Diyarbakır). The Koçali Complex consists of two different units: the volcano–sedimentary unit (Tarasa and Konak Formations) and the Koçali Ophiolite (Beyarslan and Bingöl, 2010; Beyarslan, 2017).

The Tarasa and Konak formations were thrust onto the Koçali Ophiolite and these units are then covred by the Upper Maastrichtian–Eocene conglomerates, sandstones, mudstones, limestones, and marl of the Arabian Plate (Beyarslan *et al*., 2016). The Tarasa volcanics and the Konak formation contain radiolarian faunas, indicating Carnian to Rhaetian age (Uzunçimen *et al*., 2011). Varol *et al*. (2011) studied the geochemistry of basic volcanics within the Tarasa volcanics and reported enriched mid–ocean ridge basalt (E–MORB) and normal mid–ocean ridge basalt (N–MORB) type sources.

The Koçali Ophiolite, which thrusts onto the Karadut Complex, consists of mantle peridotites, gabbros, sheeted dikes, ultramafic, and mafic dikes, plagiogranite, basaltic pillow lavas, and isolated diabase dikes (Beyarslan, 2017). Serpentinised harzburgites in the mantle contain some small podiform chromitite pods. The cumulate mafic rocks of the Koçali Ophiolite are characterised by interlayered gabbros and isotropic gabbros. The contact between mantle peridotite and cumulate gabbros is generally sharp, but a thin dunitic transition zone is observed in some places (Beyarslan, 2017).

2.3- Bitlis and Pütürge massifs

The Bitlis–Pütürge massifs are regional–scale allochthonous units and show similar stratigraphic successions. Yılmaz and Yiğitbaş (1991) interpreted the Bitlis–Pütürge massifs as being a once–united giant tectono–stratigraphic unit disrupted and fragmented during orogeny. They comprise a high–grade metamorphic basement and a lower–grade metamorphic cover, forming an envelope around the core (Göncüoğlu and Turhan, 1984; Erdem, 1994;

Erdem and Bingöl, 1995; Bingöl *et al*., 2015; Beyarslan, 2017), and stratigraphically overlain by the Middle Eocene Maden Complex or Late Miocene to Quaternary volcanics, in the north. They have thrust onto the neo–autochthonous Arabian Plate and ophiolites along their southern contacts.

The high–grade metamorphic basements of the two massifs are similar and are composed of granitoid gneiss (augen gneiss – metagranite) ranging in composition from quartz diorite, tonalite to granodiorite, various schists, amphibolites, and meta–granite. Bingöl *et al*. (2015) and Beyarslan *et al*. (2016) indicated that the base of the Pütürge massif is Neoproterozoic–Early Cambrian aged at 544–551 Ma. From the Ediacaran–Early Cambrian metagranites in the Bitlis massif, Ustaömer *et al*. (2009, 2012) obtained a 207Pb/206Pb single–zircon age of 545 Ma, as well as obtaining an age of 531 Ma from Mutki metagranites and an age of 572 Ma from Doğanyol metagranites in the Bitlis Massif.

The basement of the Bitlis massif underwent high–grade metamorphism, possibly related to a collision during the final amalgamation of exotic terranes with northeast Gondwana or to the development of a subsequent subduction zone along the margin of Gondwana (Collins and Pisarevsky, 2005). The basement is overlain by sedimentary rocks containing mid–Devonian fossils that were metamorphosed under greenschist and at low–T/high–P conditions, much lower than the metamorphic grade of the basement (Göncüoğlu and Turhan, 1984). In the Pütürge massif, the basement units are overlain by Middle Eocene sedimentary and volcanic rocks of Maden Complex (Erdem and Bingöl, 1995: Yiğitbaş and Yılmaz, 1996). Tourmaline bearing micro–leucogranite occurs as large tectonic lenses immediately above the autochthonous Maden complex sediments in Çakçak Tepe (Yazgan and Chessex, 1991). These kinds of the tourmaline–bearing leucogranites associated with high–grade metamorphic rocks occur in the Higher Himalayas and postdate the main compressional phase due to continental collision (Gansser, 1964; Le Fort, 1981; Vidal *et al*., 1982). The Triassic rocks characteristics of the Bitlis massif are missing in the Pütürge massif. The Triassic unit consists of recrystallised limestones and calc–schists grading upward into metashales, metatuffs, metadiabases, metabasalts and finally metaconglomerates, metamudstones, and shales (Oberhansli *et al*., 2012).

The basement rocks and cover unit Bitlis–Pütürge massifs were metamorphosed under greenschist facies conditions during the Late Cretaceous (Yazgan and Chessex, 1991; Erdem and Bingöl, 1995; Oberhansli *et al*., 2012).

2.4- Maden complex

The unit was first named the “Maden unit” by Rigo de Righi and Cortesini (1964). In previous studies that have been carried out in different parts of the SE Anatolian Orogenic Belt, the Maden Complex was named “Maden complex” (Perinçek and Özkaya, 1981; Yazgan, 1983, 1984; Yazgan *et al*., 1983; Aktaş and Robertson, 1984; Hempton, 1985), “Baykan complex” (Sungurlu, 1974), “Karadere formation” (Açıkbaş and Baştuğ, 1975; Aktaş and Robertson, 1984), “Maden formation” (Özkaya, 1982; Çağlayan *et al*., 1984; Michard *et al*., 1984) and “Maden group” (Erdoğan, 1977; Aktaş and Robertson, 1984). According to Aktaş and Robertson (1984), the Maden complex essentially consists of Upper Cretaceous ophiolitic rocks, Lower Tertiary sedimentary rocks, and some volcanic rocks. They accepted that the Maden complex is a composite tectono–stratigraphic unit. The group of Middle Eocene–aged volcanic and sedimentary rocks was named the Maden group “sensu stricto” by these researchers. The Maden group begins with basal clastics accompanied alkaline basaltic lavas (Yılmaz *et al*., 1987; Yiğitbaş *et al*., 1993). In the Maden–Ergani region, Erdoğan (1982) included all the sedimentary and volcanic rocks of this study in his “Maden group” and suggested a simple stratigraphy comprised of a lower volcanic–sedimentary unit and an upper volcanic unit (Fig. 2). In the Pütürge–Kale region, Açıkbaş and Baştuğ (1975) distinguished four different units in the Maden complex: the Ceffan formation, the Arbo formation, the Melefan formation and the Karadere formation. The Ceffan formation, constitued the basal unit of the Maden complex and unconformably overlies the Precambrian–Permian Pütürge Metamorphics and Late Cretaceous Guleman ophiolites. This formation consists of basal conglomerates at the base and medium–to thin bedded sandstone.

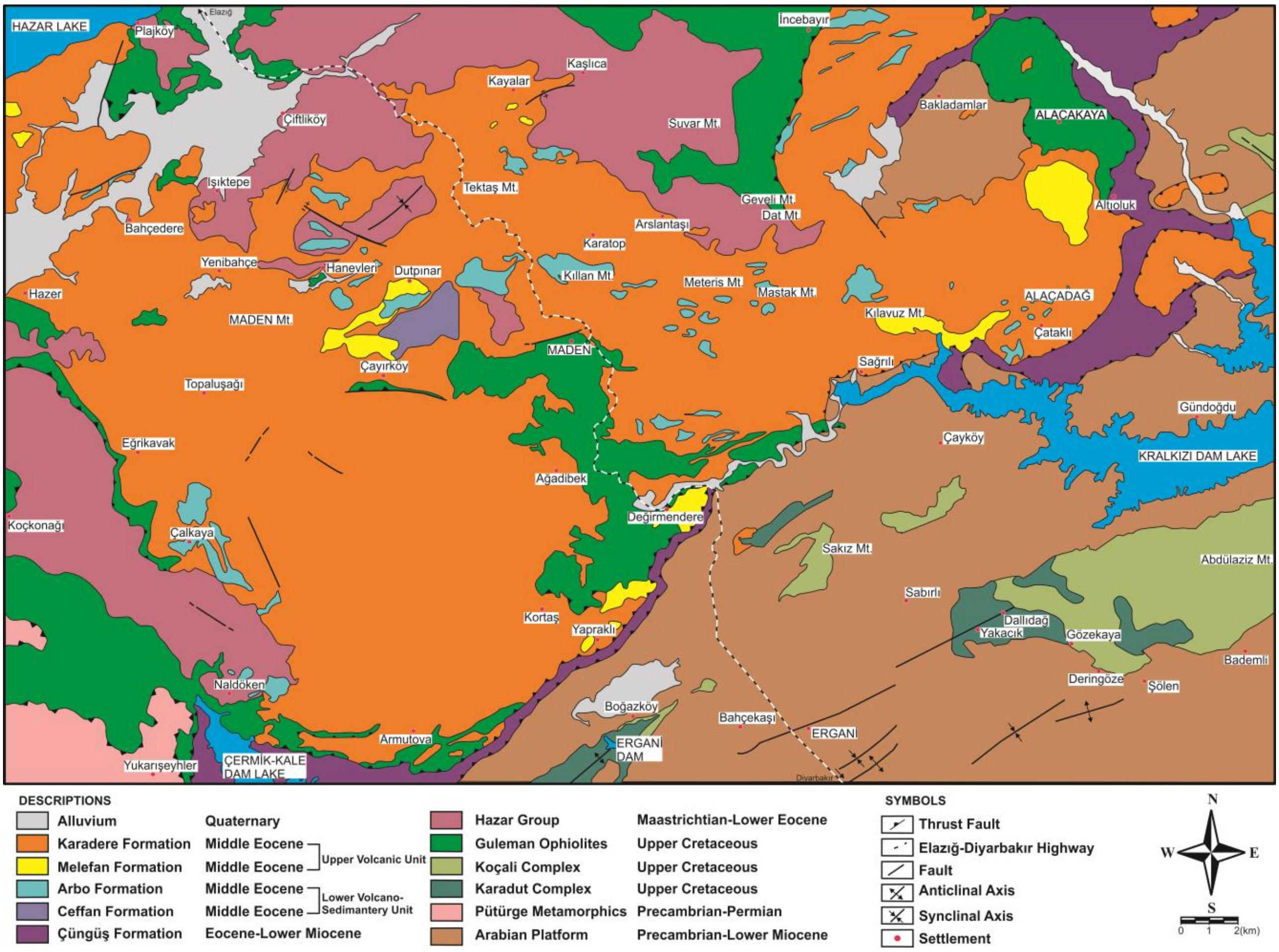

Figure 2) Geological map of the Ergani–Maden region (simplified from MTA, 2011).

The upper part consists of sandy limestone and shale intercalation. The Arbo formation conformably overlies the Ceffan formation. The formation is composed of limestone with abundant nummulite fossils. The upper part of the formation contains rhyolite and tuff (Robertson *et al.*, 2007). The Melafan formation, conformably overlies the Arbo formation. The formation consist of pelagic limestones intercalated with radiolarite, chert and spilitic lavas reddish–coloured mudstones, in place, interfinger with spilitic volcanics or overly these rocks (Şaşmaz *et al.*, 2014). The Karadere formation conformably overlies the Melafan formation and is tectonically overlain by Elazığ magmatics and ophiolites. The Karadere formation comprises basalts and andesites and also contains pyroclastics and sub–volcanic rocks (Fig. 3). Aktaş and Robertson (1984) included the Ceffan formation with the Gehroz and the Simaki formations in the Upper Palaeocene–Eocene Hazar group. The equivalents of the Hazar group are reported to be Maastrichtian to Middle Eocene in the Malatya and Palu (east of Elazığ) areas (Perinçek, 1979; Yazgan, 1981).

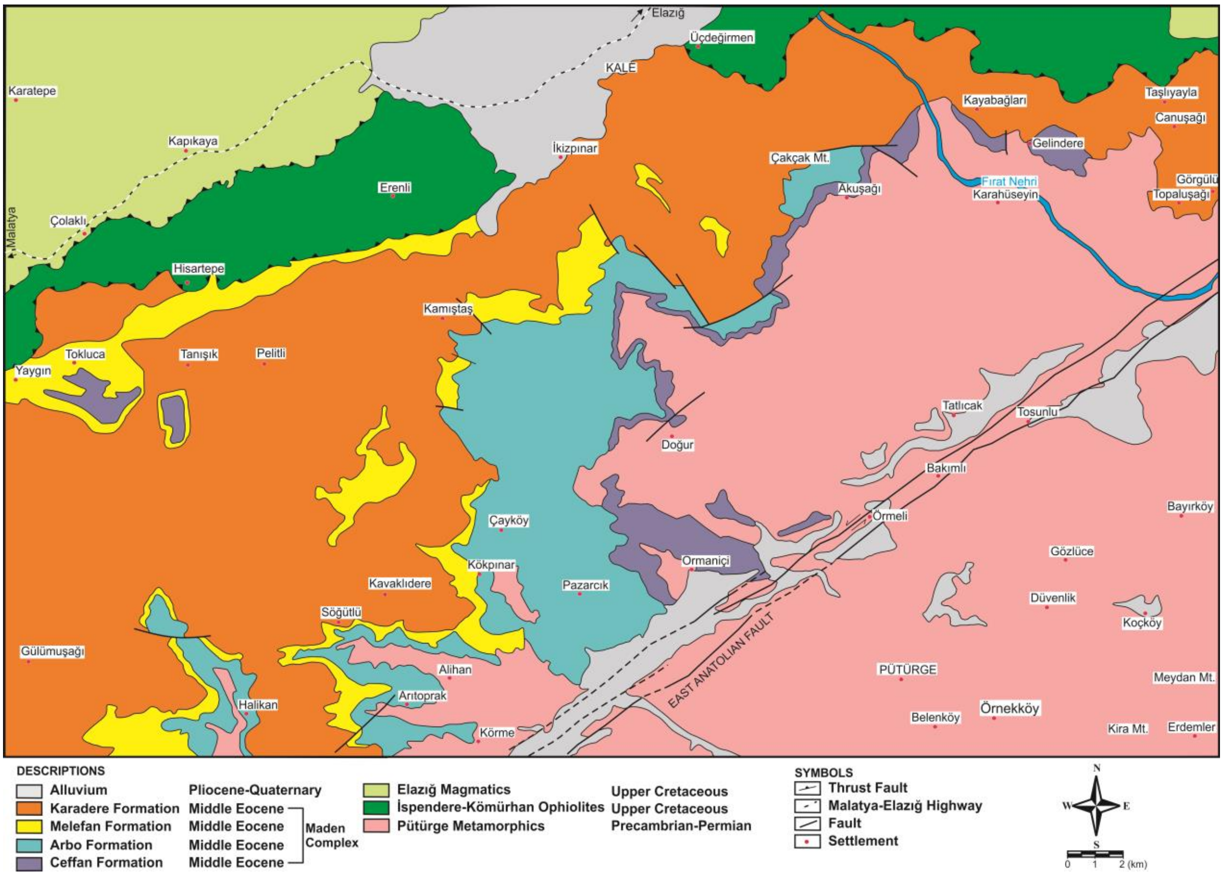

Figure 3) Geological map of the Kale–Pütürge region (simplified from MTA,1986).

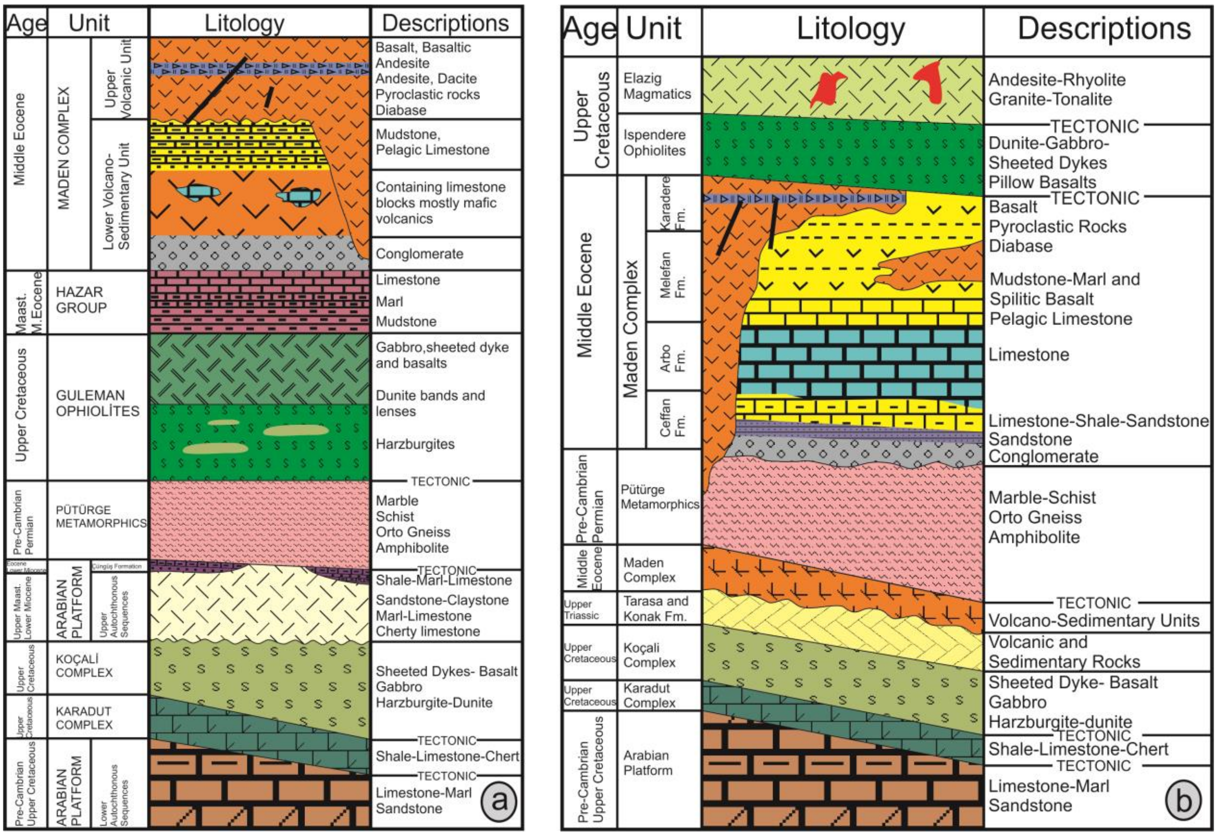

Figure 4a) Tectono–stratigraphic columnar section of the Ergani–Maden area, (b) Tectono–stratigraphic columnar section of the Kale–Pütürge area.

The Maden complex outcrops two different tectono–stratigraphic positions in the studied areas: (1) in the suture zone beneath the Bitlis–Pütürge massifs and (2) on the Pütürge massif and the Guleman ophiolite. It mainly outcrops to the south of Elazığ in the Maden–Ergani region and to the southeast of Malatya (between Pütürge–Kale) (Figs. 4a, b).

In the Maden–Ergani region, the Upper Cretaceous Guleman ophiolite and the Maastrichtian–Lower Eocene Hazar group thrust over the Maden Complex. In contrast, in the Pütürge–Kale region, the Maden Complex is located between the Precambrian–Permian Pütürge massif and the Late Cretaceous İspendere ophiolite. The Maden complex unconformably overlies the Pütürge Massif, whereas the İspendere Ophiolite thrusts over the Maden Complex (Yazgan, 1983; Beyarslan, 1991).

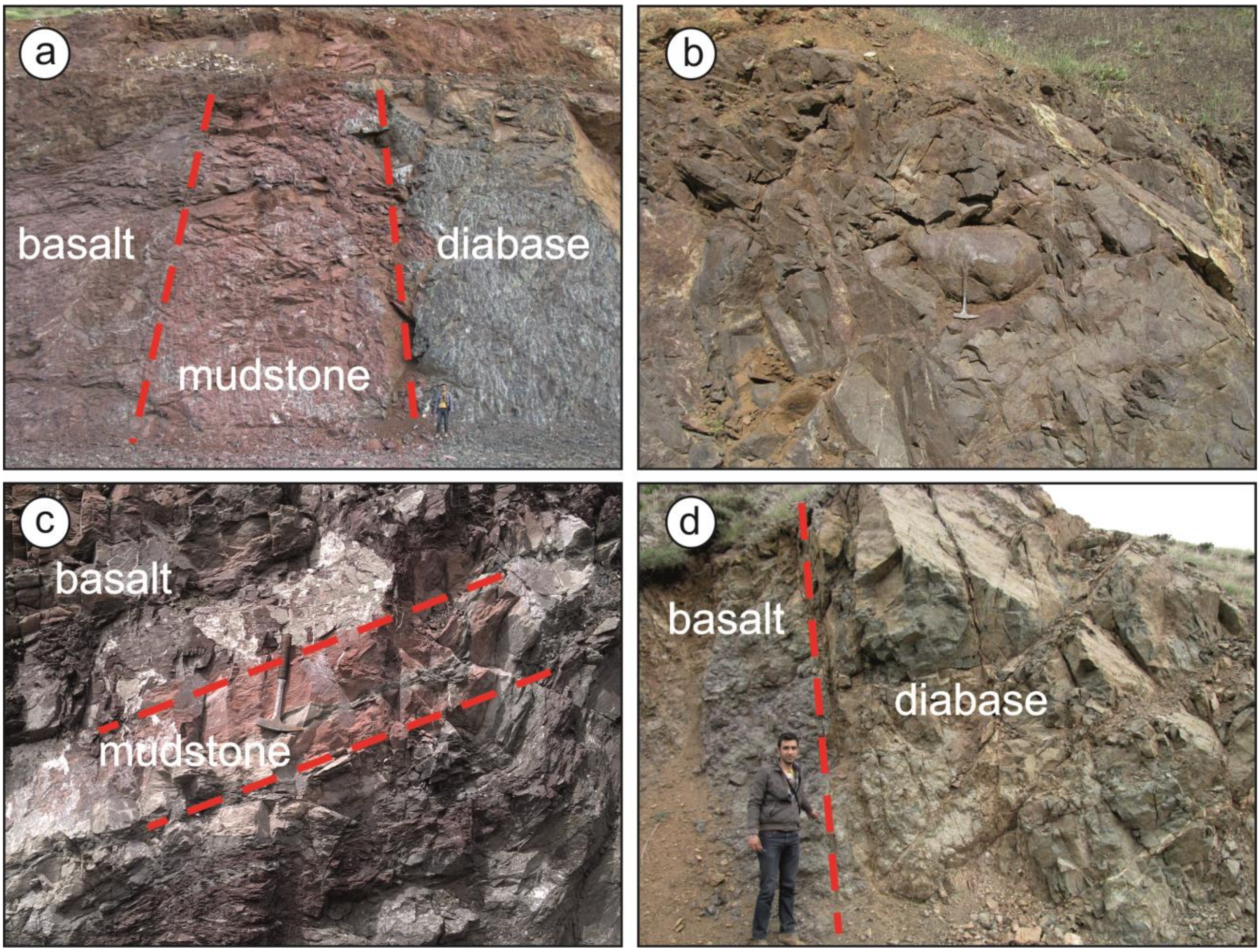

Figure 5a) The lateral–vertical transitive relationship between the red colored basalts of the Maden complex and the reddish colored mudstone and the greenish colored diabase dike, (b) Ellipsoidal shaped pillow basalts belonging to the Maden complex, (c) Red colored mudstones intercalated with volcanics belonging to the Maden complex, (d) A greenish diabase dike that cuts the basalts of the Maden complex.

The Maden Complex begins with basal clastics. Upwards, green sandstone, silicified red chert, and red coloured mudstones become dominant. The higher part of the Maden Complex consists of massive limestone blocks and red coloured pelagic carbonates interbedded with bioclastic material. According to Aktaş and Robertson (1984), the pelagic carbonates and bioclastic materials are all re–deposits, rather than in situ carbonate build–ups. The Maden complex contains basalts, basaltic andesite, andesite, dacite, diabase, and pyroclastic rocks, which are intercalated and lateral–vertical transitive with all of these sedimentary successions (Fig. 5a). The brecciation is widespread due to extensive tectonism. Additionally, intensive alterations can be observed in the region, depending on the thrusts and imbrications. Basalts largely crop out in the study area. They are generally greenish, brownish and bearded in appearance, and include massive, ellipsoidally–shaped pillow lavas, and broken pillow basalts (Fig. 5b). Basalts are intercalated mainly with red cherts and red mudstones (Fig. 5c). Andesites and basaltic andesites are more greyish in color compared to basalts, and though, macroscopically it is difficult to distinguish them from basalts. It is, however, possible to make this distinction based on petrographical and geochemical features. The dacites are macroscopically lighter, grey, whitish and darker than the mafic volcanics. Dykes of diabases of variable thickness often cut through basalts and are greenish in color, medium grained (Fig. 5d). In the study area, pyroclastic rocks are represented by agglomerate, lapillistone and tuff. The agglomerates are composed of bombs and the volcanic parts are welded by a cement material. The lapillistones have a basic and andesitic composition, whereas the tuffs are finely grained. Some andesitic and dacitic dykes belonging to the Maden Complex cut through the upper part of the Pütürge massif (Yıldırım, 2010).

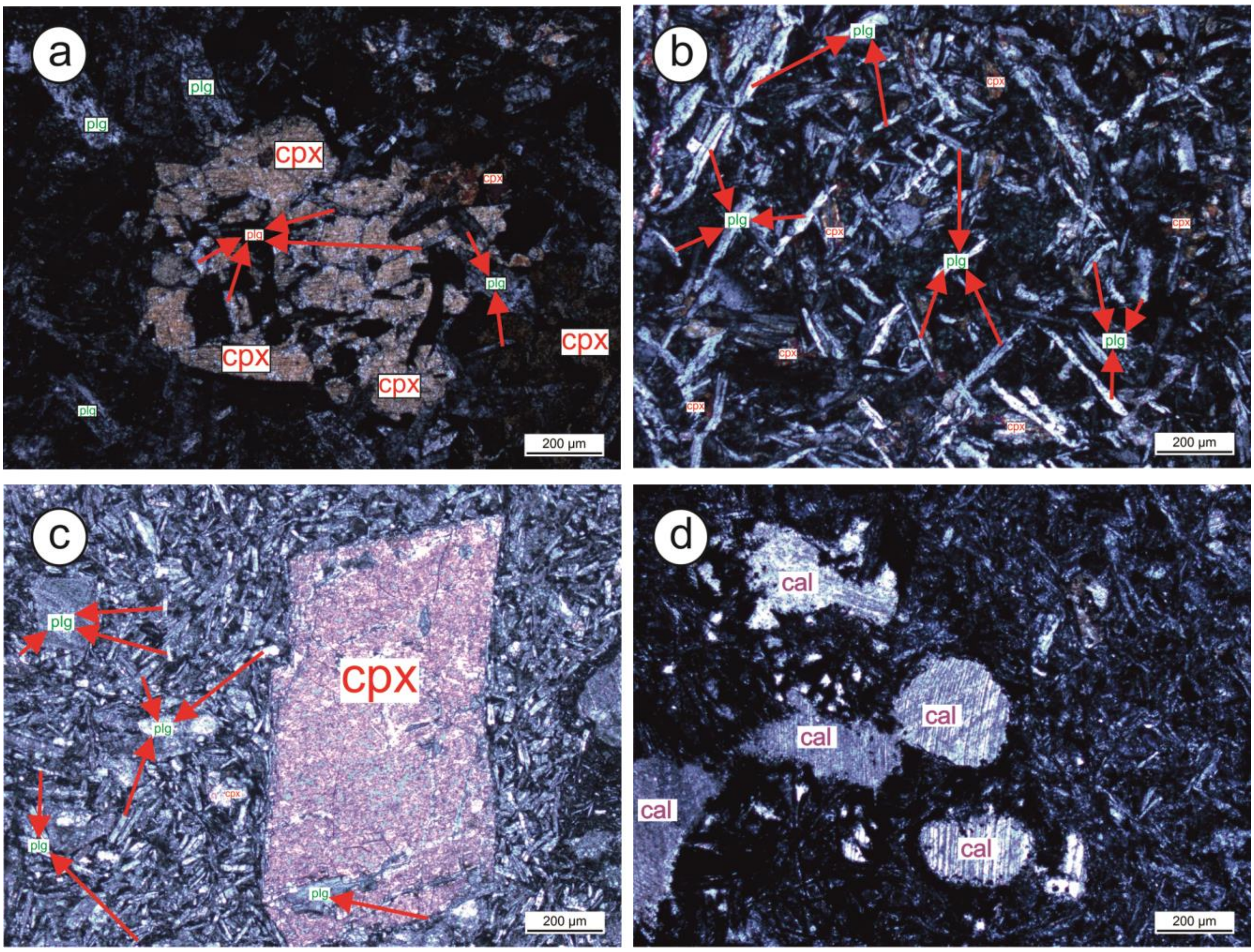

Figure 6) Photomicrographs (cross–polarized light) of the volcanic rocks of Maden complex, (a) ophitic texture in basalt, (b) intersertal texture in andesite, (c) porphyric texture in basalt, (d) amygdaloidal texture in basalt (plg: plagioclase, cpx: clinopyroxene, cal: calcite, chl: chlorite).

According to previous work (e.g. Özkaya, 1978; Perinçek, 1979; Yazgan, 1981; Aktaş and Robertson, 1984; Sungurlu *et al*., 1985), the age of the Maden Complex is Middle Eocene. Pişkin and Delaloye (1981) obtained a K–Ar ages ranging from 45±5.7 to 52.0±10.3 Ma for pillow lavas and diabase of the Karadere formation. In agreement with this, Yiğitbaş and Yılmaz (1996) reported Middle Eocene planktonic foraminifera in the pelagic limestones of the Maden group. They also observed that these pelagic sedimentary rocks are intercalated with transitional or tholeiitic basaltic lavas.

3- Analytical methods

Thirty–nine representative samples of volcanic rocks from the Maden complex have been analysed for their major–trace–rare earth element compositions (Table 1) at the Lab of Department of Geosciences, National Taiwan University, where major elements were measured by X–ray fluorescence (XRF) techniques on fused glass beads using a Rigaku® RIX–2000 spectrometer and trace elements were measured by the inductively coupled plasma–mass spectrometry (ICP–MS) using an Agilent 7500cs equipment. The detailed analytical procedures were same as those reported in Lin *et al*. (2012).

4- Petrography

The volcanic rocks of the Maden complex are represented essentially by massive and pillowed basalt, massive andesite, pyroclastic rocks, subordinately diabase and dacite. They display ophitic, porphyric, intersertal, spherulitic, amygdaloidal textures with varying mineralogy (Fig. 6). The basalts are macroscopically gray, dark blackish gray and sometimes greenish depending on the degree of chloritization and epidotization and display ophitic, intersertal, spherulitic and porphyritic textures. The basalts contain plagioclase, clinopyroxene, less olivine and Fe–Ti oxides. Plagioclase is present either as phenocryst phase or as microlites. The groundmass containing plagioclase microlites is often pervasively altered. The clinopyroxene phenocrysts are augites. The amygdaloidal texture is also observed in some samples, where vesicles are filled with calcite, quartz, celadonite and zeolite minerals. The andesites contain plagioclase, hornblende and Fe–Ti oxides. Andesites have porphyritic texture with plagioclase and hornblende in phenocrysts. Most phenocrysts in these rocks exhibit subhedral form. Plagioclase phenocrysts show albite and carlspad twinning or normal zoning. Dacites generally display porphyritic texture with plagioclase, biotite and occasionally quartz phenocrysts. When pyroclastic rocks are examined according to grain size, they are composed of tuffs, lapilli–stones and agglomerates. All volcanic rocks are strongly altered. Secondary phases are epidote, calcite, chlorite, quartz.

5- Whole Rock Analysis

5.1- Rock classification

The K_2O–SiO_2 diagram of Peccerillo and Taylor (1976) is used to classify of the volcanic rocks of the study area. As shown in Fig. 7 most samples plot in the calc–alkaline and low–K tholeiitic areas, whereas some basaltic and basaltic andesite samples plot in the high–K calc–alkaline and shoshonitic areas. The dominant rocks are calc–alkaline and low–K tholeiitic basalt and andesite.

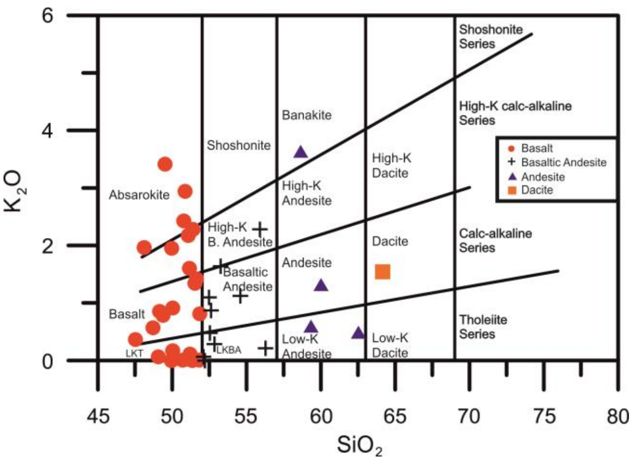

Figure 7) A diagram of K_2O versus SiO_2 showing rock classification of Maden Complex rocks (boundaries and fields after Peccerillo and Taylor, 1976). LKT = low–K tholeiite, LKBA = low–K basaltic andesite.

Table 1) Major and Trace element data for Middle Eocene Maden Complex, SE Turkey.

Rock Type	Basalt	Basalt	Basalt	Basalt	Basalt	Basalt	Basalt	Basalt	Basalt	Basalt	Basalt	Basalt	Basalt
Sample	26MA	39MA	65MA	80MA	95MA	97MA	98MA	102MA	114MA	115MA	04PTR	26PTR	27PTR
Latitude (°N)	38.4489	38.4601	38.4150	38.3884	38.4597	38.4521	38.4341	38.3507	38.3220	38.3088	38.2567	38.2498	38.2616
Longitude (°E)	39.6263	39.6411	39.6097	39.5522	39.6188	39.6246	39.6399	39.6633	39.6394	39.6535	38.6279	38.6558	38.5604
Major oxides (wt %)													
SiO_2	49.54	48.77	45.52	48.34	49.14	49.91	48.11	48.78	46.53	49.17	50.19	48.10	48.37
TiO_2	1.06	1.91	0.78	1.62	1.05	1.07	1.43	1.3	2.03	0.79	1.70	1.25	0.86
Al_2O_3	18.52	18.01	18.37	14.74	18.12	15.40	18.71	19.64	15.60	16.63	17.56	18.58	16.26
$Fe_2O_3^a$	6.64	12.4	11.34	11.61	8.15	12.35	11.32	11.72	12.64	8.41	10.76	9.10	8.74
MnO	0.15	0.41	0.14	0.26	0.13	0.15	0.18	0.13	0.2	0.15	0.18	0.13	0.31
MgO	8.84	5.64	5.53	8.06	5.86	7.38	4.78	5.00	6.51	6.71	2.11	2.58	8.53
CaO	5.80	3.14	11.48	6.69	7.86	4.92	7.7	2.85	7.22	7.79	6.54	9.25	8.65
Na_2O	4.1	5.9	2.12	4.94	5.56	6.07	4.18	3.37	3.75	4.39	6.31	5.03	3.51
K_2O	1.29	0.89	0.35	0.17	0.02	0.11	0.77	2.82	1.9	2.1	1.38	1.88	0.01
P_2O5	0.2	0.4	0.15	0.19	0.21	0.14	0.25	0.29	0.34	0.14	0.49	0.37	0.16
LOI	4.43	3.77	4.64	4.33	4.42	3.39	3.42	4.72	3.50	4.52	3.80	5.17	5.66
Sum	100.57	101.25	100.42	100.95	100.53	100.88	100.84	100.61	100.22	100.79	101.02	101.43	101.06
Mg#[b]	72.49	47.38	49.1	57.88	58.75	54.21	45.53	45.77	50.51	61.27	27.93	35.97	65.91
Trace elements (ppm)													
P	861	1624	578	763	864	528	1014	1258	1316	582	1921	1503	664
Sc	26.2	30.8	32.8	27.8	34.4	41.6	49	31.7	44.4	22.6	29.8	28.3	23
Ti	6084	10100	4648	8501	5981	5770	7982	7240	11070	4524	9111	7206	4825
V	244.4	144.6	285.5	266.8	265.2	247.3	370.3	178.7	291.1	253.2	267.7	237.9	225.8
Cr	177	309	294	111	170	199	57	42	66	416	160	61	410
Mn	1090	2880	1073	1761	983	1004	1294	937	1451	1144	1215	1021	2137
Co	33.2	59.2	36.7	33.6	23.4	31.6	32.3	38.3	37.4	31.3	30.3	21.9	33.8
Ni	86.82	153.6	127.1	51.95	75.63	95.82	44.63	49.4	41.73	185.5	109.2	47.68	168.9
Cu	92.16	256.1	53.63	121.3	34.62	29.08	82.79	17.7	24.22	78.08	24.63	25.02	16.87
Zn	162.9	207.8	73.6	72.8	6.5	72.6	73.3	108	102.7	104.2	95.4	54.2	77
Ga	18.1	16.9	15.8	15.3	18.1	13.8	20.4	17	19.1	15.6	20.1	18.7	13.7
Rb	18.67	18.82	7.54	2.72	1.08	1.52	14.22	48.22	38.47	30.19	43.2	32.42	0.75
Sr	454	172	416	157	133	114	758	276	215	405	173	514	300
Y	24.3	42.7	15.8	29.1	25	22	32.1	32.5	39.4	19.4	34.7	27.5	18.6
Zr	101	123	49	93	101	56	106	91	132	57	108	137	61
Nb	3.4	6	1.4	6.8	3.5	2.7	3.8	3.7	8.6	2.3	18.3	5.6	2.4
Cs	0.25	0.40	0.46	0.82	0.09	0.04	0.41	1.67	0.90	0.59	2.14	0.57	0.08
Ba	114	78	93	47	38	24	167	103	165	214	171	298	18
La	9.3	12.7	7.3	7.3	9.6	4.2	12.3	10.6	9.2	6.9	36	14.1	7.8
Ce	22.4	20.1	16.5	17.3	22.5	9.9	29.3	22.6	23.2	14.9	65.9	31.6	17.2
Pr	3.11	3.61	2.32	2.44	3.12	1.45	4.04	3.31	3.36	2.03	7.58	4.27	2.38
Nd	14.15	17.56	10.74	11.87	14.29	7.31	18.44	15.61	16.68	9.25	29.36	18.92	10.83
Sm	3.48	4.7	2.64	3.47	3.57	2.34	4.64	4.28	5.1	2.41	5.88	4.49	2.72
Eu	1.20	1.65	0.89	1.23	1.17	0.78	1.51	1.48	1.65	0.85	1.84	1.48	0.87
Gd	3.86	6.19	2.7	4.54	3.83	3.22	5.15	5.05	6.32	2.86	5.89	4.73	2.96
Tb	0.65	1.00	0.44	0.78	0.65	0.57	0.85	0.85	1.07	0.48	0.95	0.75	0.49

Table 1) Continued.

Dy	4.11	6.55	2.79	4.98	4.09	3.67	5.47	5.3	6.88	3.13	5.81	4.68	3.14
Ho	0.87	1.38	0.58	1.03	0.87	0.79	1.15	1.12	1.42	0.67	1.19	0.96	0.65
Er	2.5	4.07	1.63	3.05	2.52	2.32	3.39	3.3	4.09	2.04	3.48	2.82	1.92
Tm	0.38	0.60	0.25	0.44	0.39	0.36	0.51	0.51	0.61	0.31	0.52	0.42	0.29
Yb	2.46	3.71	1.6	2.82	2.51	2.29	3.33	3.13	3.75	2.01	3.21	2.73	1.87
Lu	0.38	0.57	0.24	0.42	0.39	0.35	0.49	0.47	0.55	0.31	0.50	0.42	0.29
Hf	2.46	3.2	1.34	2.48	2.41	1.56	2.77	2.36	3.48	1.54	2.74	2.97	1.59
Ta	0.22	0.39	0.08	0.43	0.21	0.15	0.24	0.25	0.54	0.13	0.73	0.38	0.13
W	0	0.16	0	0.05	0	0.11	0.10	0	0.09	0.04	0.64	0.02	0.02
Tl	0.18	0.90	0.04	0.09	0	0.02	0.53	0.78	0.52	0.57	0.57	0.60	0.02
Pb	2.09	2.09	1.37	2.19	0.97	1.45	2.42	2.4	2.47	2.61	2.75	0.95	2.23
Th	1.06	0.6	0.96	0.68	1.02	0.52	1.82	1.27	1	0.89	5.1	1.47	1.06
U	0.43	0.46	0.17	0.2	0.35	0.17	0.59	0.42	0.41	0.19	0.83	0.44	0.36

[a]Total iron as Fe_2O_3.

[b]Mg# = [molar 100 × Mg/(Mg + Fe^{+2})]

Table 1) Continued.

Rock Type	Basalt	Basalt	Basalt	Basalt	Basalt	Basalt	B. And.	B. And.	B. And.	B. And.	B. And.	B. And.	B. And.
Sample	31PTR	32PTR	39PTR	41PTR	01ISP	04ISP	36MA	38MA	47MA	72MA	112MA	02SN	31MA
Latitude (°N)	38.2205	38.1950	38.2589	38.2658	38.3970	38.3959	38.4650	38.4608	38.4731	38.4153	38.3327	38.0502	38.4533
Longitude (°E)	38.5580	38.5844	38.6213	38.5654	38.7735	38.7791	39.6586	39.6512	39.6060	39.5747	39.6338	38.3312	39.6361
Major oxides (wt %)													
SiO_2	47.95	50.20	47.29	47.55	49.20	46.83	50.32	51.63	50.56	52.99	50.59	51.77	54.74
TiO_2	2.11	2.40	1.88	0.97	0.97	0.58	1.1	1.48	0.74	1	1.14	1.17	0.91
Al_2O_3	14.83	15.17	15.47	17.29	21.48	18.85	18.87	17.38	14.46	17.16	18.36	17.21	13.44
Fe2O3[a]	13.59	12.32	13.06	9.02	9.24	6.59	7.49	10.20	10.79	7.99	9.64	9.92	7.69
MnO	0.17	0.28	0.18	0.13	0.18	0.12	0.17	0.15	0.14	0.14	0.15	0.17	0.08
MgO	7.18	6.48	5.21	9.17	4.34	8.01	5.57	3.99	7.06	3.75	6.29	5.98	6
CaO	6.62	4.99	7.31	6.38	6.85	11.88	5.83	6.60	9.04	9.86	5.54	5.91	3.78
Na_2O	3.34	5.59	5.67	2.06	2.19	2.66	6.74	5.75	2.88	2.92	3.46	3.29	3.14
K_2O	0	0	0.07	3.28	1.54	0.55	0	0.28	0.46	1.09	1.06	1.60	3.40
P_2O5	0.22	0.31	0.24	0.17	0.18	0.08	0.32	0.26	0.11	0.18	0.18	0.19	0.17
LOI	4.87	3.17	4.79	4.87	4.57	4.00	4.59	3.25	4.71	3.18	4.09	3.18	5.53
Sum	100.87	100.91	101.16	100.90	100.75	100.15	100.98	100.96	100.94	100.26	100.50	100.38	98.87
Mg#[b]	51.12	51.03	44.15	66.81	48.19	70.65	59.55	43.64	56.46	48.19	56.40	54.43	60.7
Trace elements (ppm)													
P	861	1263	1009	668	746	371	1334	1070	439	760	707	834	666
Sc	38.2	32.9	26.5	42.8	30.2	46.7	16.7	37.2	25.8	30.2	32.3	58.4	21.1
Ti	11420	12910	10240	5529	5515	3359	6204	8186	4026	5970	6230	6784	4752
V	367.6	281.5	377.2	250.5	230.6	147.6	161.3	371.7	259.7	211.4	260.6	289.8	108.3
Cr	77	28	41	309	40	333	117	186	288	50	55	103	186
Mn	1235	2055	1323	983	1290	875	1243	1076	936	1105	1086	1299	548
Co	38.7	30.4	36.1	34.2	26.8	26	26.1	23.9	35	23.1	26.4	26.5	19.5
Ni	50.44	20.5	36.9	139.2	49.6	126.9	64.92	119	128.5	43.49	41.36	63.79	108.8
Cu	55.45	5.75	58.21	9.57	34.09	40.56	112.7	134.1	28.24	57.15	66.65	35.32	7.64
Zn	170.4	55.1	82.8	60.6	68.9	37.2	34.1	93.1	53	53.8	53.3	64.5	45.2
Ga	20	19.2	22.8	15.9	18.8	14.1	23.2	22.2	13	17.6	16.8	18.8	10.3
Rb	0.32	0.43	1.51	54.44	39.95	11.57	0.27	4.69	6.05	15.73	17.91	29.03	20.19
Sr	132	89	92	156	484	622	121	513	147	428	257	430	207

Table 1) Continued.

Y	36.9	46.7	38.3	20.1	25.5	13.3	23.9	30.8	16.1	28	24.7	27.5	15.8
Zr	114	140	120	68	71	35	128	111	33	101	99	79	66
Nb	7.3	7.6	7.4	2.6	2.2	1.4	14	3.9	1.5	2.4	2.1	2.5	3.2
Cs	0.16	0.07	0.38	0.78	0.89	0.44	0.03	0.23	0.55	0.28	0.4	0.68	0.34
Ba	20	30	89	220	100	54	23	144	37	239	135	242	167
La	8.1	8.9	14.5	9	10.8	3.6	17.5	13.2	3.7	12.5	8.5	9.1	6.2
Ce	19.9	22.9	30.4	20.3	21.5	8.2	37.9	30.1	8.3	27.5	20.8	21.7	13.4
Pr	2.86	3.40	3.98	2.75	3.09	1.18	4.74	4.22	1.12	3.76	2.88	3.05	1.94
Nd	14.04	17.30	18.19	12.42	14.03	5.74	19.88	19.17	5.45	16.86	13.41	14.35	8.96
Sm	4.36	5.49	5.05	3.01	3.49	1.65	4.29	4.65	1.67	4.01	3.51	3.71	2.32
Eu	1.61	1.49	1.72	0.99	1.19	0.61	1.36	1.52	0.64	1.32	1.14	1.26	0.8
Gd	5.68	7.09	6.23	3.3	3.93	2.03	4.33	5	2.32	4.34	3.95	4.3	2.69
Tb	0.98	1.22	1.04	0.54	0.66	0.35	0.68	0.84	0.41	0.72	0.65	0.71	0.44
Dy	6.37	7.95	6.55	3.43	4.15	2.24	4.07	5.27	2.73	4.52	4.15	4.56	2.78
Ho	1.33	1.66	1.35	0.71	0.88	0.47	0.84	1.11	0.56	0.96	0.86	0.96	0.58
Er	3.91	4.9	3.93	2.09	2.59	1.38	2.41	3.19	1.66	2.81	2.54	2.82	1.68
Tm	0.59	0.73	0.58	0.31	0.40	0.2	0.36	0.48	0.25	0.44	0.38	0.43	0.25
Yb	3.7	4.58	3.66	1.99	2.54	1.32	2.37	3.02	1.56	2.81	2.47	2.76	1.65
Lu	0.55	0.68	0.54	0.3	0.38	0.2	0.37	0.45	0.23	0.43	0.37	0.42	0.25
Hf	3.08	3.68	3.23	1.71	1.86	0.94	2.99	2.86	1.01	2.58	2.37	2.1	1.72
Ta	0.44	0.47	0.39	0.16	0.14	0.09	0.91	0.24	0.08	0.16	0.15	0.15	0.2
W	0.15	0.43	0.22	0	0	0	0	0.05	0.02	0	0	0.01	0.09
Tl	0	0	0.42	0.59	0.54	0	0.01	0.20	0.17	0.18	0.38	0.54	0.38
Pb	3.18	0.65	1.79	1.41	2.52	0.5	2.84	3.28	1.17	5.51	5.59	1.52	2.59
Th	1.05	0.96	2.27	1.17	1.51	0.4	2.16	1.86	0.39	1.73	1.06	1.24	0.72
U	0.27	0.3	0.6	0.39	0.29	0.13	0.7	0.73	0.12	0.66	0.7	0.39	0.42

[a]Total iron as Fe_2O_3.

[b]Mg# = [molar 100 × Mg/(Mg + Fe^{+2})]

Table 1) Continued.

Rock Type	Andesite	Andesite	Andesite	Dacite	Diabase	Diabase	Diabase	Diabase	Diabase	Diabase	Diabase	Diabase	Diabase
Sample	54MA	87MA	13TK21	73MA	32MA	44MA	45MA	51MA	85MA	109MA	116MA	37PTR	38PTR
Latitude (°N)	38.4283	38.3820	38.4304	38.4152	38.4526	38.4712	38.4736	38.4252	38.3825	38.3471	38.3088	38.2591	38.2604
Longitude (°E)	39.6442	39.5834	39.6299	39.5747	39.6368	39.6429	39.6448	39.6479	39.5634	39.6515	39.6535	38.5734	38.6225
Major oxides (wt %)													
SiO_2	57.58	60.92	57.44	62.96	49.83	54.77	54.47	49.37	49.87	49.89	51.32	49.21	47.34
TiO_2	1.11	0.8	0.98	0.94	0.99	1.31	1.38	1.06	1.17	0.73	0.88	1.14	1.09
Al_2O_3	14.58	16.17	16.86	15.93	18.85	17.07	17.40	17.79	16.29	15.94	19.38	17.02	16.04
$Fe_2O_3{}^a$	10.33	5.64	7.66	5.76	7.37	8.86	9.04	9.62	8.99	7.84	8.6	7.92	10.34
MnO	0.17	0.17	0.07	0.09	0.19	0.11	0.11	0.22	0.12	0.13	0.22	0.13	0.16
MgO	6.65	3.38	4.87	1.48	9	3.97	3.09	8.43	7.92	5.80	4.39	7.21	6.2
CaO	1.95	4.69	4.88	4.17	3.29	5.23	4.59	3.8	6.09	11.93	5.72	8.95	10.06
Na_2O	2.16	4.95	3.26	5.02	5.84	5.57	4.89	3.42	4.77	3.89	6.06	2.84	4.01
K_2O	1.27	0.48	0.58	1.52	0.06	0.21	2.23	2.19	0.78	0.01	0.85	2.36	0.83
P_2O5	0.15	0.21	0.2	0.27	0.22	0.24	0.26	0.16	0.16	0.12	0.13	0.14	0.27
LOI	4.89	2.64	3.45	2.21	5.13	3.56	2.82	5.13	3.82	4.63	3.16	3.15	4.34
Sum	100.83	100.06	100.25	100.34	100.76	100.89	100.26	101.18	99.98	100.89	100.71	100.07	100.66
Mg#[b]	56.03	33.69	54.28	55.74	70.77	47.01	40.32	63.45	63.56	59.43	50.24	64.31	54.28
Trace elements (ppm)													
P	593	846	798	1140	934	1008	1071	644	643	483	524	532	1134
Sc	32.8	28.9	37	22.3	27.5	34.4	23	26.5	37.7	31.6	45.6	65.5	29
Ti	6343	4455	5665	5356	5609	7369	7609	5461	6680	4109	5053	6666	6330
V	152.6	63.92	261.9	48.49	165.6	295.4	283.1	226.9	277.7	226.7	269	327.7	263.5

Table 1) Continued.

Cr	298	18	17	6	127	65	17	76	190	111	41	222	77
Mn	1239	1226	571	703	1343	803	784	1428	894	897	1596	1021	1233
Co	41.3	7.2	14.3	7.4	31	20.1	17.8	23.5	32.2	25.6	23.6	26.3	35.5
Ni	223.5	11.09	16.3	5.83	86.44	42.61	22.58	53.11	73.79	53.94	43.59	79.21	47.07
Cu	72.43	27.94	42.66	13.37	93.97	81.69	43.46	50.87	97.39	27.78	56.72	65.8	90.02
Zn	98.6	72.3	319.4	81	83	67.6	26.9	61.6	67.7	46	79.2	45.6	65.7
Ga	17.6	17.9	14.2	19	18.8	20.2	19.1	16.2	17	15.2	17.4	15.7	18.2
Rb	47.98	7.91	10.27	15.06	1.44	2.28	21.04	15.23	12.19	1.23	9.41	36.74	9.27
Sr	181	463	366	286	450	264	537	272	232	207	254	299	274
Y	21.6	35.7	23.2	42.2	19.4	27.3	32.9	20.6	22.1	17.5	23.2	20.8	25.4
Zr	122	132	82	209	88	109	139	90	66	49	68	65	89
Nb	23.3	4.2	3.2	4.5	10.5	4.9	5.9	2.9	4.8	1.8	2	3.3	17.6
Cs	2.19	0.31	0.48	0.16	0.05	0.06	0.53	0.28	0.28	0.03	0.07	0.66	0.37
Ba	80	118	158	398	33	68	428	220	45	14	135	399	370
La	23	14.6	12	21.2	11	13.4	13.7	10.3	7.1	4.4	6.3	6.7	36.3
Ce	48.6	32.8	25.4	46.6	23.9	29.4	31.4	23.3	15.7	10.1	14.8	15.5	65.2
Pr	5.34	4.50	3.51	6.26	3.04	3.92	4.26	3.21	2.13	1.43	2.08	2.12	6.87
Nd	20.8	20.74	15.01	27.4	13.19	17.5	19.09	14.24	9.83	6.86	9.73	9.96	25.62
Sm	4.24	5.38	3.62	6.34	3.02	4.15	4.64	3.39	2.76	1.99	2.72	2.71	4.75
Eu	1.16	1.69	1.09	1.84	0.95	1.35	1.49	1.12	0.97	0.71	0.97	0.96	1.48
Gd	4.16	5.89	3.84	6.69	3.25	4.34	5.01	3.5	3.31	2.51	3.37	3.23	4.5
Tb	0.64	0.99	0.61	1.10	0.52	0.73	0.84	0.55	0.59	0.43	0.57	0.54	0.72
Dy	3.83	6.33	3.85	6.87	3.26	4.61	5.42	3.38	3.81	2.87	3.72	3.47	4.32
Ho	0.79	1.33	0.87	1.48	0.68	0.98	1.16	0.7	0.81	0.62	0.81	0.73	0.89
Er	2.23	3.84	2.51	4.31	1.98	2.83	3.39	2.04	2.32	1.87	2.44	2.19	2.56
Tm	0.34	0.58	0.39	0.67	0.3	0.43	0.52	0.31	0.35	0.29	0.38	0.32	0.37
Yb	2.13	3.77	2.63	4.41	1.95	2.81	3.43	1.96	2.21	1.85	2.4	2.05	2.4
Lu	0.32	0.57	0.40	0.67	0.30	0.43	0.51	0.31	0.33	0.29	0.38	0.31	0.36
Hf	3	3.46	2.04	5.15	2.11	2.75	3.47	2.16	1.83	1.36	1.82	1.69	2.09
Ta	1.42	0.26	0.2	0.31	0.68	0.3	0.37	0.18	0.27	0.11	0.13	0.2	0.69
W	0.31	0	0.17	0	0	0	0	0.02	0	0.09	0.2	0.01	0.13
Tl	0.76	0.11	0.06	0.41	0	0.07	0.4	0.36	0.03	0.08	0.23	0.52	0.2
Pb	6.41	2.83	1.93	3.64	0.89	1.55	0.84	2.65	0.72	1.52	2.76	1.18	2.3
Th	4.18	1.73	2.03	3.39	1.52	1.57	1.94	1.45	0.97	0.55	0.79	0.79	4.9
U	0.95	0.42	0.66	1.12	0.52	0.53	0.66	0.4	0.28	0.21	0.28	0.28	1.32

[a]Total iron as Fe_2O_3.

[b]Mg# = [molar 100 × Mg/(Mg + Fe^{+2})]

5.2- Chemical features of the Maden Complex rocks

Whole rock data for the studied samples are listed in Table 1. The samples have variable SiO_2 (45.52–62.96 wt.%), TiO_2 (0.58–2.40 wt.%), Al_2O_3 (13.44–21.48 wt.%), Fe_2O_3 (5.64–13.59 wt.%), MgO (1.48–9.17 wt.%), CaO (1.95–11.93 wt.%), Na_2O (2.06–6.74 wt.%), K_2O (0.01–3.40), Ti (3359–12910 ppm), Ni (5.83–223 ppm), Rb (0.27–54.4 wt.%), Sr (89–758 ppm), Mg# (27.9–72.5), La/Yb (1.83–15.13) and relatively stable MnO (0.07–0.41 wt.%), P_2O_5 (0.08–0.49 wt.%). All samples have high LOI varying from 2.21 to 5.66 wt.%, indicating the effect of alteration.

Chondrite–normalized REE patterns of the different volcanic rocks of the Maden complex show similar trends. They have enrichment in LREE and show relatively flat patterns from Tb to Lu (Fig. 8). They display slightly negative Eu anomalies suggesting the rocks evolved by fractional crystallization of plagioclase or an origin from partial melting in the presence of feldspar in the source.

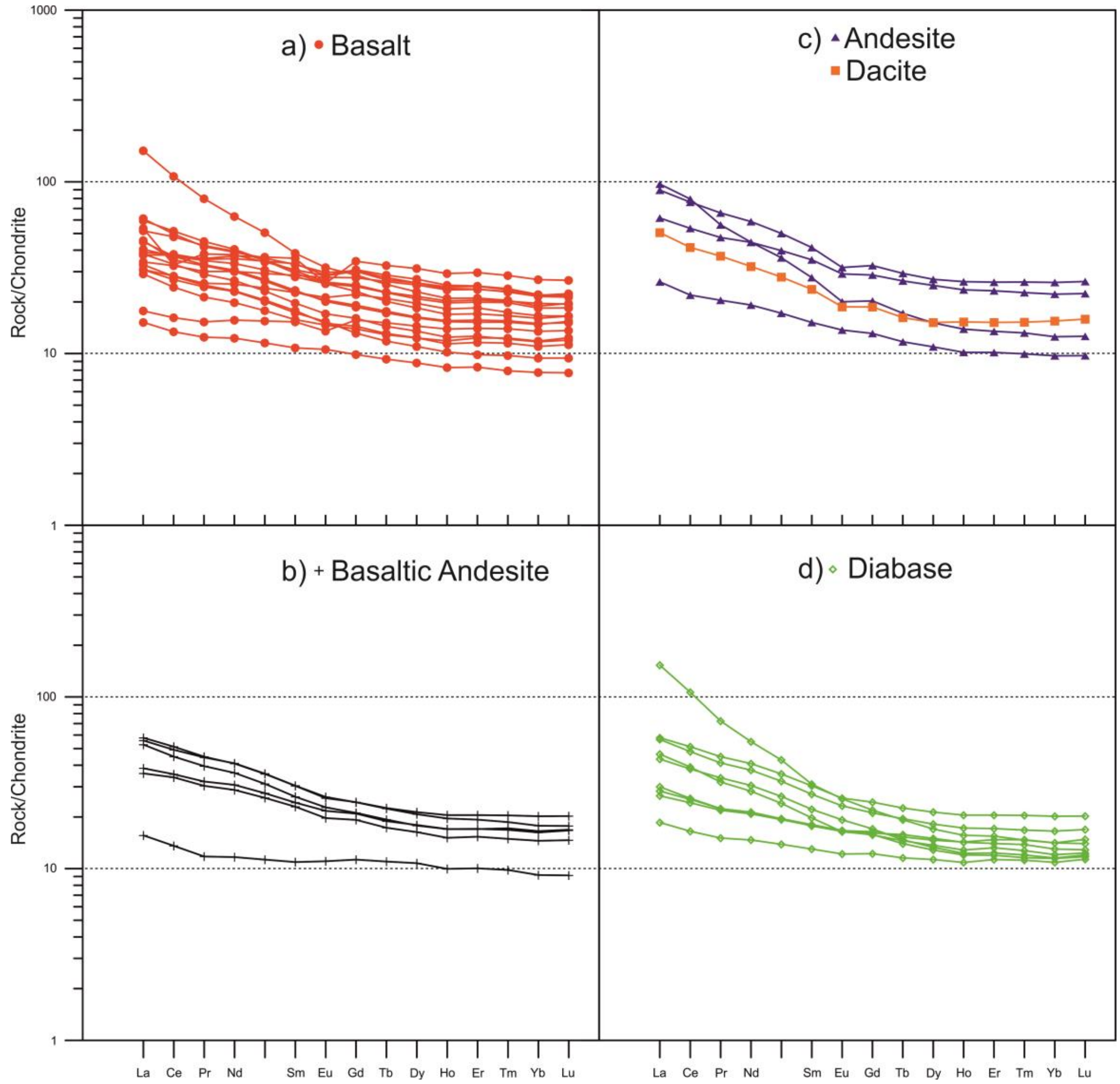

Figure 8) Chondrite (CI)–normalized spidergrams and N–MORB normalized trace element plots for Middle Eocene Maden complex. Normalizing values are after Sun and McDonough (1989).

On the N–MORB normalized incompatible element spider diagrams, the volcanic rocks of the Maden complex display an enrichment of overall Large Ion Lithophile Elements (LILE) and light REE, with negative Nb, Ta, and Ti, and positive Pb anomalies (Fig. 9).

6- Discussion

The volcanics of the Maden complex display negative Nb and Ta anomalies, positive P anomalies and negative Zr–Hf anomalies relative to Sm and Nd. The negative Nb and Ta anomalies and positive Pb anomalies indicate that these kinds of volcanics are an island arc volcanics and continental crustal rocks (Zou *et al*. 2000). The negative Zr–Hf anomalies relative to Sm and Nd are also commonly observed in upper continental crustal rocks (Rudnick and Gao, 2003) and subduction–related magmas (Gill, 1981; Pearce and Peate, 1995; Tatsumi, 1989).

Magmas formed in orogenic belts show Nb–Ta trough and enrichments in large ion lithophile elements (LILE), Th, Pb, Sr and K in primitive mantle normalized trace element variation diagrams (Lustrino and Wilson, 2007). According to Pearce and Norry (1979), there are considerable variabilities in Zr/Nb among oceanic basalts, i.e. OIB (<10), E–MORB (~10) and N–MORB (~40).

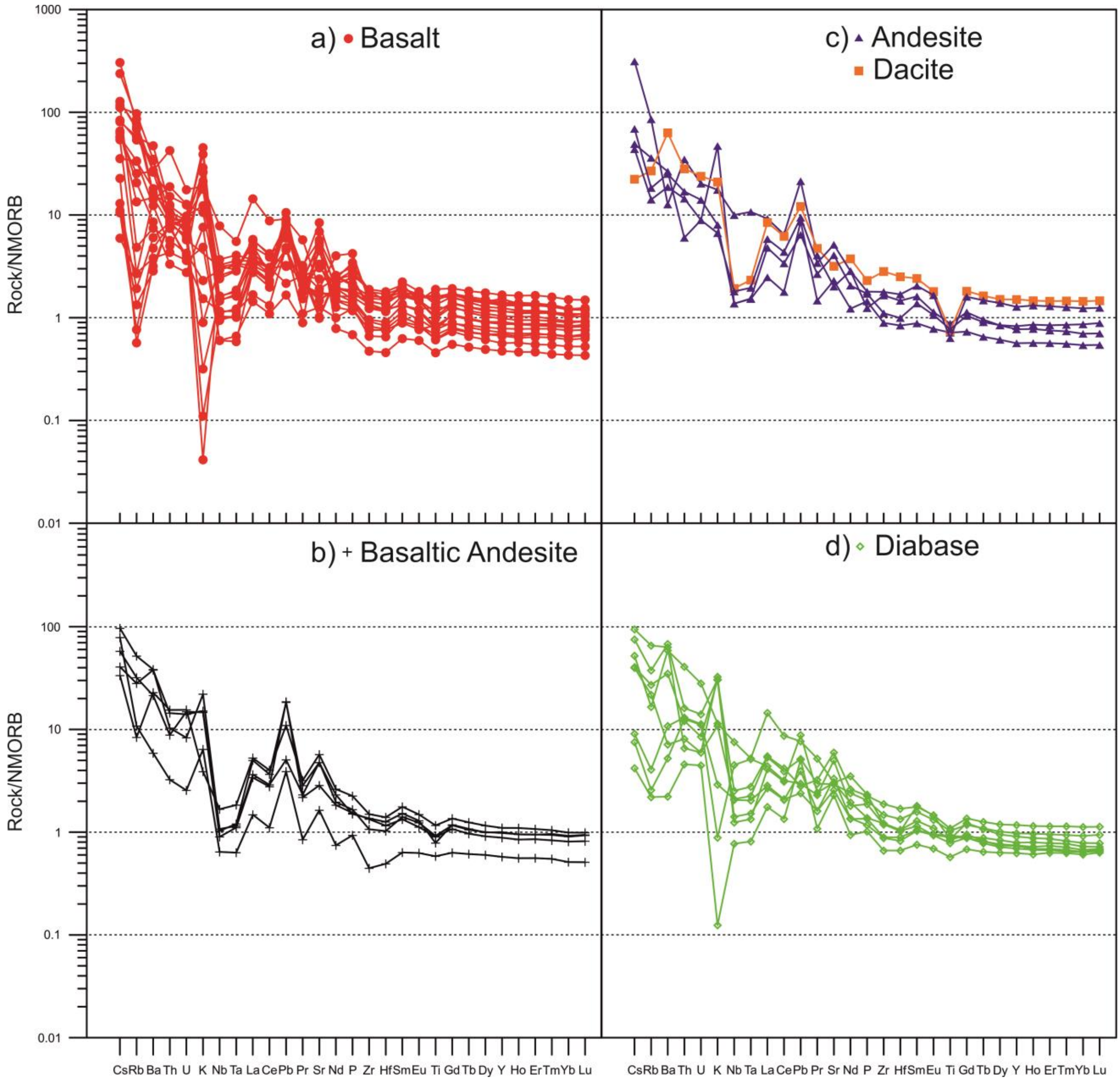

Figure 9) N–MORB normalized trace element plots for Middle Eocene Maden complex. Normalizing values are after Sun and McDonough (1989).

The Zr/Nb of the basalt, basaltic andesite and andesite samples of the samples analysed ranges from 5.06 to 47.14, consistent with derivation from N–MORB and E–MORB–like source. On the diagrams of Nb/Yb or Zr/Yb versus Ta/Yb, the samples plot between the average N–MORB and E–MORB composition (Fig. 10). Such geochemical character is commonly interpreted in three different ways. It might reflect magma genesis in a recent subduction–related setting (Gill, 1981), in sources that had undergone supra–subduction zone metasomatism (Aldanmaz *et al*., 2000; Seghedi and Downes, 2011), or crustal contamination of mantle–derived magmas (Harangi *et al*., 2006).

Due to its complex structure, the different relations between the Maden complex and the older units, limited geochemical data from volcanics, there are many geodynamic models to explain the formation of the Maden complex. Rigo de Righi and Cortesini (1964) suggested that "Maden unit" were formed in a synorogenic "back–deep"–type basin. Erdoğan (1982) suggested an immature island arc origin for the rocks of the Maden complex excluding the ophiolitic rocks.

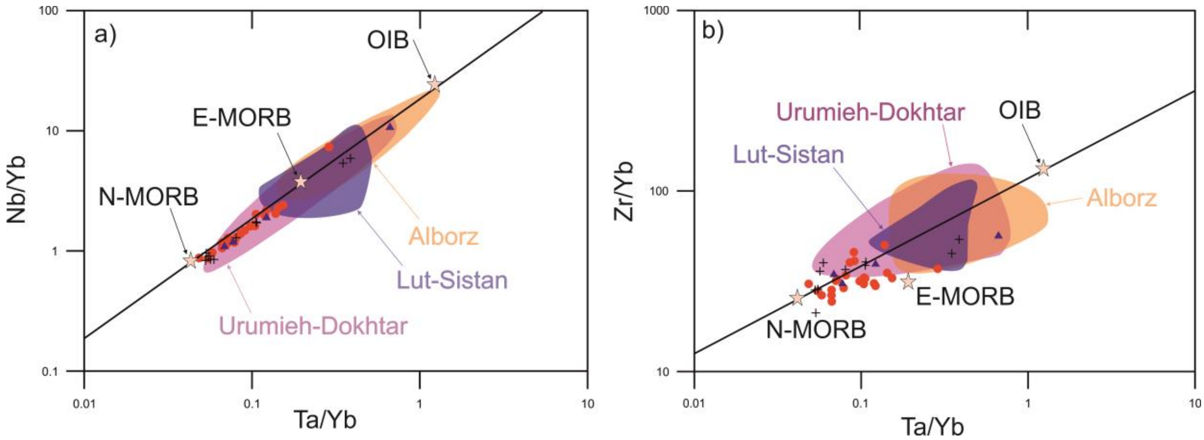

Figure 10) Binary diagrams of incompatible element ratios illustrating the mantle source feature for the SE Turkey Eocene magmatic rocks, (a) Nb/Yb versus Ta/Yb, (b) Zr/Yb versus Ta/Yb. N–MORB, E–MORB and OIB values are after Sun and McDonough (1989). Solid lines denote mantle arrays extrapolated from N–MORB and OIB values. Inset shows data for Eocene–Oligocene magmatic rocks from the Urumieh–Dokhtar region, southwestern Iran (Ahmadian et al., 2009; Omrani et al., 2008; Verdel et al., 2011), the Alborz region, northern Iran (Aghazadeh et al., 2010, 2011; Asiabanha and Foden, 2012; Asiabanha et al., 2012), Lut–Sistan region, eastern Iran (Pang et al., 2013). Symbols are the same as Figure 6.

His proposal was mainly based on limited geochemical data from lavas which apparently possessed island–arc tholeiitic compositions. Baştuğ (1980) concluded that intercontinental collision occurred in the Late Cretaceous and that the Maden complex (of this study) represents the products of a new phase of rifting which took place in Eocene time. Perinçek and Özkaya (1981) suggested that the "Maden complex" represents a marginal basin formed behind the arc related with a south–dipping subduction zone. Similarly, Şengör and Yılmaz (1981) suggest that the Maden complex formed in a back–arc basin. Yazgan (1981) however suggests that the Maden complex volcanics were erupted in response to the underthrusting of the Arabian Plate below the Pütürge massif metamorphics, in collisional tectonics which produced lavas of calc–alkaline affinities. In contrast, Aktaş and Robertson (1984) suggest that the Karadere formation (volcanics of the Maden complex) formed by rifting of the forearc, possibly related to oblique convergence in the Middle Eocene.

Comparisons can thus be made with other areas exhibiting evidence of subduction, collision and related magmatism, sedimentation and tectonics, for example, in Iran. There are many similarities between the Eocene volcanism in Turkey and the Eocene–Oligocene volcanism in Iran.

Pang *et al*. (2013) proposed a geodynamic model to explain the tectono–magmatic evolution of the Eocene–Oligocene post–collisional magmatism in the Lut–Sistan region, eastern Iran. This model can be applied to explain the formation of the Eocene Magmatism (the Maden complex) in the Southeastern Anatolian orogenic belt. The generation of the Eocene Maden complex volcanism can be explained as follow: (1) the South branch of the Neo–Tethys was opened between the Arabia plate and the Anatolian micro–plate in Upper Triassic (Perinçek 1979; Şengör and Yılmaz, 1981; Beyarslan and Bingöl, 2000). This ocean continued to spreading with a production of MORB materials through a well–developed mid–oceanic ridge during Late Triassic–Early Cretaceous. (2) An inter–oceanic subduction towards north was begun in the Late Cretaceous. (3) Closure of the southern branch of the Neo–Tethys and collision of the Arabian micr–plate with Arabian Plate and emplacement of the ophiolite and Pütürge massif onto the Arabian Plate in Late Maastrichtian (Fig. 11).

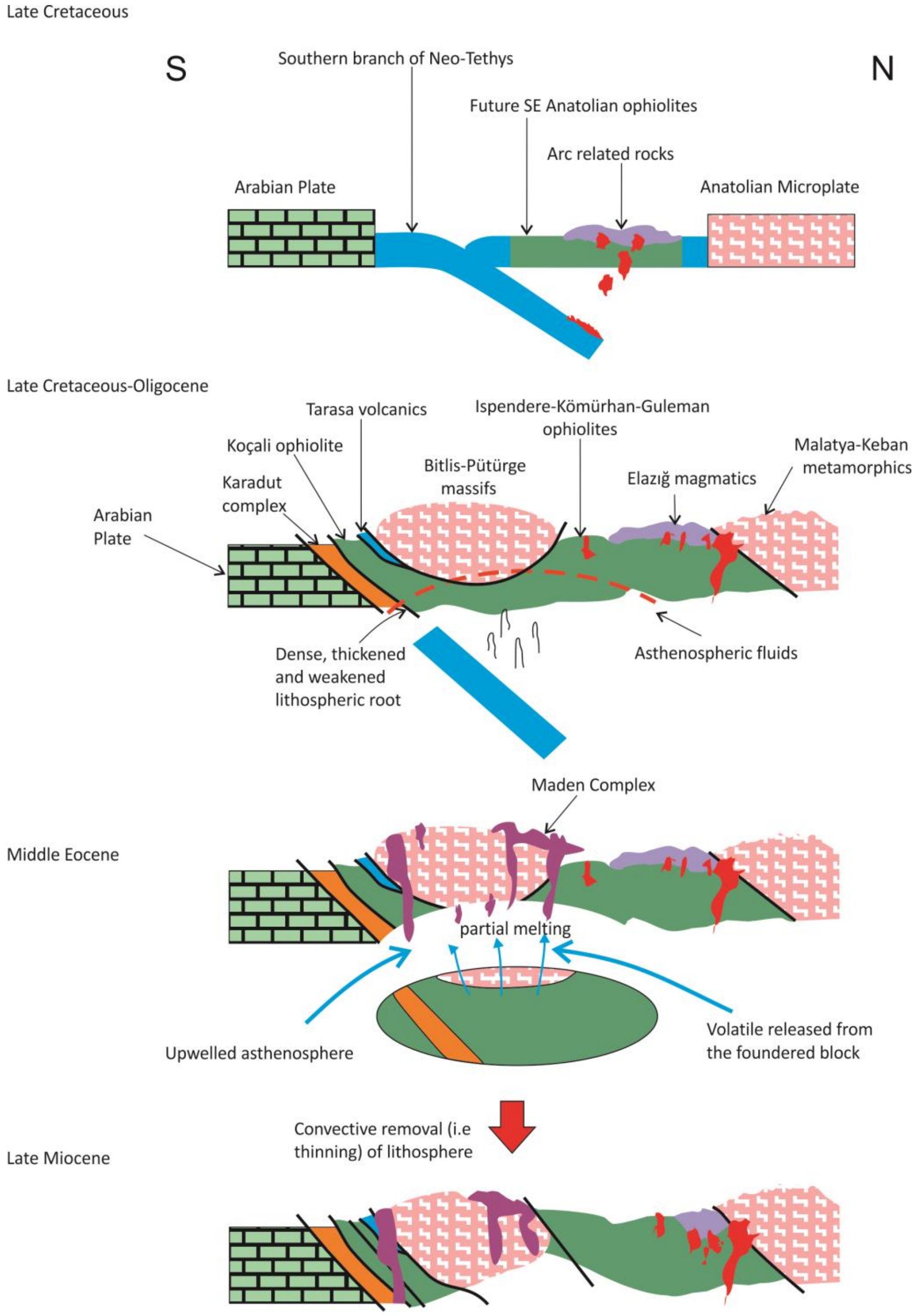

Figure 11) Geodynamic model for the tectonic and magmatic evolution of the Bitlis–Zagros suture zone, SE Turkey.

This collision occurred in Late Cretaceous, as evidenced by the emplacement of 74–72 Ma collisional monzodiorite and monzonite pluton in suture zone (Lin *et al*., 2015). (4) Crustal thickining and gravitationally unstability of the north of Arabian Plate detachement from the remnant lithosphere by convective thinning (Fig. 11). (5) The adiabatic upwelling of the asthenosphere triggered heating and melt generation in the subduction–modified mantle. (6) Formation of the Eocene magmatism onto the Pütürge metamorphics and the Late Cretaceous ophiolites.

7- Conclusion

Middle Eocene magmatic rocks crop out in a large area in the Southeast Anatolian orogenic belt, SE Turkey. These magmatic rocks are mainly basalts, andesites and subordinate dacites. There are also some diabase dykes cutting the basalts and andesites. Most of the basalts and andesites have low–K tholeiite and calc–alkaline affinity, but some of them consist of high–K calc–alkaline and shoshonitic rocks. The K–Ar ages data of Pişkin and Delaloye (1981) indicate that the magmatism was active during the Middle Eocene (~50 to ~45 Ma). The magmas display an orogenic signature. HFSE and heavy REE ratios point to an N–MORB and an E–MORB–like mantle source. In view of available geological and geochemical observations, the magmatism can best be explained by lithospheric removal and asthenospheric upwelling associated with an extensional collapse of the SE Turkey.

Acknowledgements

This study was supported by a Scientific Research Project from Fırat University (Project No: MF 1402), and a TÜBİTAK–2214A (Scientific and Technical Research Council of Turkey International Research Fellowship Programme).

References

Açıkbaş, D., Baştuğ, C. 1975. V. Bölge Cacas–Hani yöresi kuzey sahalarının jeoloji raporu ve petrol olanakları, TPAO Rapor No: 917.

Aghazadeh, M., Castro, A., Omran, N. R., Emami, M. H., Moinvaziri, H., Badrzadeh, Z. 2010. The gabbro–(shoshonitic)–monzonite–granodiorite association of Khankandi pluton, Alborz Mountains, NW Iran. Journal of Asian Earth Sciences: 38, 199–219.

Aghazadeh, M., Castro, A., Badrzadeh, Z., Vogt, K. 2011. Post–collisional polycyclic plutonism from the Zagros hinterland: the Shaivar Dagh plutonic complex, Alborz belt, Iran. Geological Magazine: 148, 980–1008.

Ahmadian, J., Haschke, M., McDonald, I., Regelous, M., Ghorbani, M. R., Emami, M. H., Murata, M. 2009. High magmatic flux during Alpine–Himalayan collision: constraints from the Kal–e–Kafı complex, central Iran. Geological Society of America Bulletin: 121, 857–868.

Aktaş, G., Robertson, H. F. 1984. The Maden Complex, SE Turkey: evolution of a Neotethyan active margin. In: Dixon, J.E., Robertson, A.H.F. (Eds.), The Geological Evolution of the Eastern Mediterranean. The Geological Society by Blackwell Scientific Publication, Oxford, London, Edinburgh, Boston, Palo Alto, Melbourne, pp. 375–401.

Aldanmaz, E., Pearce, J. A., Thirlwall, M. F., Mitchell, J. G. 2000. Petrogenetic evolution of late Cenozoic, post–collision volcanism in western Anatolia, Turkey. Journal of Volcanology and Geothermal Research: 102, 67–95.

Asiabanha, A., Bardintzeff, J.M., Kananian, A., Rahimi, G., 2012. Post–Eocene volcanics of the Abazar district, Qazvin, Iran: mineralogical and geochemical evidence for a complex magmatic evolution. Journal of Asian Earth Sciences 45, 79–94.

Asiabanha, A., Foden, J. 2012. Post–collisional transition from an extensional volcanosedimentary basin to a continental arc in the Alborz Ranges, N–Iran. Lithos 148, 98–111.

Baştuğ, M. C. 1980. Sedimentation, deformation, and melange emplacement in Lice basin, Dicle–Karabegan area, Southeast Turkey: The Department of Geological Engineering of the Middle East Technical University these of Doctor of Philosophy, pp. 282.

Beyarslan, M. 1991. İspendere (Kale–Malatya) ofiyolitlerinin petrografik özellikleri, Firat University, Institute of Science and

Technology, Master Thesis, Elazığ–Turkey, 56 pp.

Beyarslan, M., 2017. Supra–subduction zone magmatism of the Koçali ophiolite, SE Turkey. Journal of African Earth Sciences: 129, 390–402.

Beyarslan, M., Bingöl, A. F. 2000. Petrology of a supra–subduction zone ophiolite (Kömürhan–Elazığ–Turkey), Canadian Journal of Earth Sciences: 37, 1411–1424.

Beyarslan, M., Bingöl, A. F., 2010. Kömürhan ve İspendere Ofiyolitleri (GD Anadolu Kuşağı, Türkiye) kümülatları içerisindeki ultramafik ve mafik kütleler. Turkish Journal of Science and Technology: 5/1, 19–36.

Beyarslan, M., Bingöl A. F. 2014. Petrology of the Ispendere, Kömürhan and Guleman Ophiolites (Southeast Turkey): Subduction Initiation Rule (SIR) Ophiolites and Arc Related Magmatics. 3rd Annual International Conference on Geological and Earth Sciences (GEOS 2014) 50–60, Singapore.

Beyarslan, M., Lin, Y.–C., Bingöl. A. F., Chung, S.–L. 2016. Zircon U–Pb age and geochemical constraints on the origin and tectonic implication of Cadomian (Ediacaran–Early Cambrian) magmatism in SE Turkey. Journal of Asian Earth Sciences: 130, 223–238.

Bingöl, A. F. 1984. Geology of the Elazıg area in the Eastern Taurus region, in International Symposium on the Geology of the Taurus Belt, Proceedings, Eds. Tekeli, O., and Göncüoğlu, M. C., 26–29 September, MTA, Ankara, s. 209–216.

Bingöl A. F., Beyarslan M., Chung S–L. 2014. The Peri–Arabian ophiolites (Turkey and Syria): Mid–Oceanic Ridge (MOR) and/or Subduction Initiation Rule (SIR) Ophiolites. Bulletini I Shkencave Gjeologjıke. Proceedings XX Congress of the Carpathian–Balkan Geological Association V.1, 4–7, Tirana–Albania.

Bingöl. A. F., Chung, S. L., Beyarslan, M., Lin, Y. C. 2015. Tectonic setting and geochronology of the Cadomian (Ediacaran) magmatism in SE Turkey. Conference: IAGR Annual Convention &12th International Conference on Gondwana to Asia, At 21–23 October 2015, Tsukuba, Japan, V: IAGR Conference Series No. 21, pp. 11–12.

Collins, A. S., Pisarevsky, S. A. 2005. Amalgamating eastern Gondwana: the evolution of the Circum–Indian Orogens. Earth–Science Reviews: 71, 229–270.

Erdem, E. 1994. Pütürge (Malatya) Metamorphitlerinin petrografik ve petrolojik özel– likleri. Ph.D. Thesis Firat Univ. Inst. of Sciences and Technology, Elazığ, Turkey. 119p. (in Turkish).

Erdem, E., Bingöl, A. F. 1995. Pütürge (Malatya) Metamorfitlerinin Petrografik Özel– likleri. F.Ü.Fen veMüh. Bilimleri Dergisi: 7, 73–85 (in Turkish).

Erdogan, B. 1977. Geology geochemistry and genesis of the sulphide deposits of the Ergani–Maden region SE Turkey, PhD Thesis, University of New Brunswick.

Erdoğan, B. 1982. Ergani–Maden Yöresindeki Güneydoğu Anadolu Ofiyolit kuşağının jeolojisi ve volkanik kayaçları. Türkiye Jeoloji Kurumu Bülteni: 25, 49–50.

Gansser, A. 1964. Geology of the Himalayas, Interscience, New York, 289 pp.

Ghienne, J. F., Monod, O., Kozlu, H., Dean, W. T. 2010. Cambrian–Ordovician depositional sequences in the Middle East: a perspective from Turkey. Earth-Science Reviews: 101, 101–146.

Gill, J. B. 1981. Orogenic Andesites and Plate Tectonics. Springer–Verlag, Berlin, Heidelberg, 390 pp.

Göncüoğlu, M. C., Kozlu, H. 2000. Early Palaeozoic evolution of the NW

Gondwanaland: data from southern Turkey and surrounding regions. Gondwana Research: 3, 315–323.

Gürsu, S., Möller, A., Göncüoglu, M. C., Köksal, S., Demircan, H., Toksoy Köksal, F. Kozlu, H., Sunal, G. 2015. Neoproterozoic continental arc volcanism at the north ern edge of the Arabian Plate, SE Turkey. Precambrian Research: 258, 208–233.

Harangi, S., Downes, H., Seghedi, I. 2006. Tertiary–Quaternary subduction processes and related magmatism in the Alpine–Mediterranean region. In: Gee, D., Stephenson, R. (Eds.) European Lithosphere Dynamics. Geological Society London, Memorial: 32, 167–190.

Hempton, M. 1985. Structure and deformation history of the Bitlis suture near Lake Hazar, SE Turkey. Geological Society of America Bulletin: 96, 223–243.

Karaoğlan, F., Koller, F., Thöni, M., Parlak, O., Klötzli, U., Parlak, O. 2012. U–Pb And Sm–Nd Geochronology Of The Kizildağ (Hatay, Turkey) Ophiolite: Implications For The Timing And Duration Of Suprasubduction Zone Type Oceanic Crust Formation In Southern Neotethys, V. Jeokimya Sempozyumu, Denizli, Türkiye, p. 1.

Karaoğlan, F., Parlak, O., Klötzli, U., Koller, F., Rızaoğlu, T. 2013a. Age and duration of intra–oceanic arc volcanism built on a suprasubduction zone type oceanic crust in southern Neotethys, SE Anatolia. Geoscience Frontiers: 4, 399–408.

Karaoğlan, F., Parlak, O., Klötzli, U., Thöni, M., Koller, F. 2013b. U–Pb and Sm–Nd geochronology of the ophiolites from the SE Turkey: implications for the Neotethyan evolution. Geodinamica Acta: 25, 146–161.

Karaoğlan, F., Parlak, O., Robertson, A., Thöni, M., Klötzli, U., Koller, F., Okay, A. İ., 2013c. Evidence of Eocene high–temperature/high–pressure metamorphism of ophiolitic rocks and granitoid intrusion related to Neotethyan subduction processes (Doğanşehir area, SE Anatolia), In: Robertson, A.H.F., Parlak, O., Ünlügenç , U.C. (Eds.), Geological Development of Anatolia and the Easternmost Mediterranean Region. Geological Society, London, Special Publications, pp. 249–272.

Karaoğlan, F., Parlak, O., Hejl, E., Neubauer, F., Klötzli, U. 2016. The temporal evolution of the active margin along the Southeast Anatolian Orogenic Belt (SE Turkey): Evidence from U–Pb, Ar–Ar and fission track chronology. Gondwana Research: 33, 190–208.

Keskin, M. 2003. Magma generation by slab steepening and breakoff beneath a subduction–accretion complex: An alternative model for collision–related volcanism in Eastern Anatolia, Turkey. Geophysical Research Letters: 30, 8046.

Keskin, M. 2007. Eastern Anatolia: A hotspot in a collision zone without a mantle plume. In: Foulger, G.R., and Jurdy, D.M., (Eds.), Plates, plumes, and planetary processes. Geological Society of America Special Paper: 430, 693–722.

Le Fort, P. 1981. Manaslu leucogranite: a collision signature of the Himalaya. A model for its genesis and emplacement. Journal of Geophysical Research: 86, 10545–10568.

Lin, I.–J., Chung, S.–L., Chu, C.–H., Lee, H.–Y., Gallet, S., Wu, G., Ji, J., Zhang, Y. 2012. Geochemical and Sr\Ndisotopic characteristics of Cretaceous to Paleocene granitoids and volcanic rocks, SE Tibet: petrogenesis and tectonic implications. Journal of Asian Earth Sciences: 53, 131–150.

Lin Y.–C., Chung S.–L., Bingöl A.F., Beyarslan M., Lee H.–Y., Yang J.–H. 2015. Petrogenesis of late Cretaceous Elazığ magmatic rocks from SE Turkey: New age and geochemical and Sr–Nd–Hf isotopic constraints. Goldschmidt, Abstracts.

Lustrino, M., Wilson, M., 2007. The circum–Mediterranean anorogenic Cenozoic igneous province. Earth–Science Reviews: 81, 1–65.

Michard, A., Whitechurch, H., Ricou, L. E., Montigny, R., Yazgan, E., 1984. Tauric subduction (Malatya–Elazığ Provinces) and its bearing on tectonics of the Tethyan realm in Turkey, in The Geological Evolution of The Eastern Mediterrranean. Eds. Dixon, J. E., Robertson, A. H. F. Geological Society of London, Special Publication: 17, 361–374.

M. T. A. 1986. 1/100.000 ölçekli Türkiye Jeoloji Haritası, Maden Tetkik ve Arama Genel Müdürlüğü, Ankara.

M. T. A. 2002. 1/500.000 ölçekli Türkiye Jeoloji Haritası, Maden Tetkik ve Arama Genel Müdürlüğü, Ankara.

M. T. A. 2011. 1/100.000 ölçekli Türkiye Jeoloji Haritası, Maden Tetkik ve Arama Genel Müdürlüğü, Ankara.

Nicoll, K. 2010. Landscape development within a young collision zone: implications for post–Tethyan evolution of the Upper Tigris River system in southeastern Turkey. International Geology Reviews: 52, 404–422.

Oberhänsli, R., Bousquet, R., Candan, O., Okay, A. 2012. Dating subduction events in East Anatolia, Turkey. Turkish Journal of Earth Sciences 21, 1–17.

Omrani, J., Agard, P., Whitechurch, H., Benoit, M., Prouteau, G., Jolivet, L. 2008. Arcmagmatism and subduction history beneath the Zagros Mountains, Iran: a new report of adakites and geodynamic consequences. Lithos: 106, 380–398.

Özkaya, İ. 1978. Ergani–Maden yöresinin stratigrafisi. Türkiye Jeoloji Bülteni 21/2, 129/139.

Özkaya, İ. 1982. Upper Cretaceous plate rupture and development of leaky transcurrent fault ophiolites in Southeast Turkey. Tectonophysics: 88, 102–116.

Pang, K.–N., Chung, S.–L., Zarrinkoub, M. H., Khatib, M. M., Mohammadi, S. S., Chiu, H.–Y., Chu, C.–H., Lee, H.–Y., Lo, C.–H. 2013. Eocene–Oligocene post–collisional magmatism in the Lut–Sistan region, eastern Iran: magma genesis and tectonic implications. Lithos: 180–181, 234–251.

Parlak, O., Rızaoğlu, T., Bağcı, U., Karaoğlan, F., Höck, V. 2009. Tectonic significance of the geochemistry and petrology of ophiolites in southeast Anatolia, Turkey. Tectonophysics: 473, 173–187.

Pearce, J. A., Peate, D. W. 1995. Tectonic implications of the composition of volcanic arc magmas. Annual Review of Earth and Plaentary Sciences: 23, 251–285.

Pearce, J. A., Norry, M. J. 1979. Petrogenetic implications of Ti, Zr, Yand Nb variations in volcanic rocks. Contrib. Mineral. Petrol. 69, 33–47.

Peccerillo, A., Taylor, S. R. 1976. Geochemistry of Eocene calc–alkaline volcanic rocks from the Kastamonu area, Northern Turkey. Contributions to Mineralogy and Petrology: 58, 63–81.

Perinçek, D. 1978. Çelikhan–Sincik–Koçali (Adımayan ili) alanının jeoloji incelemesi ve petrol olanaklarının araştırılması, Doktora Tezi, İstanbul Üniversitesi, İstanbul, 212s.

Perinçek, D. 1979. Palu–Karabegan–Elazığ–Sivrice–Malatya alanının jeolojisi ve petrol imkanları. TPAO, Ankara, Rap. No: 1361.

Perinçek, D., Özkaya, İ. 1981. Arabistan levhası kuzey kenarının tektonik evrimi. Yerbilimleri: 8, 91–101.

Pişkin, Ö., Delaloye, M. 1981. Pétrologie et géochronologie des ophiolites de Çelikhan (Taurus oriental, Turquie). Schweizerische

Mineralogische und Petrographische Mitteilungen: 61, 133–145.

Rigo de Righi. M., Cortesini, A. 1964. Gravity tectonics in foothills structure belt of southeast Turkey. American Petroleum Geology Bulletin: 48, 1911–1937.

Rizeli, M. E., Beyarslan, M., Wang, K.–L., Bingöl, A. F. 2016. Mineral chemistry and petrology of mantle peridotites from the Guleman ophiolite (SE Anatolia, Turkey): Evidence of a forearc setting. Journal of African Earth Sciences: 123, 392–402.

Robertson, A., Boulton, S. J., Taslı, K., Yıldırım, N., İnan, N., Yıldız, A., Parlak, O. 2016. Late cretaceous–Miocene sedimentary development of the Arabian continental margin in SE Turkey (Adıyaman region): implications for regional palaeogeography and the closure history of Southern Neotethys. Journal of Asian Earth Sciences: 115, 571–616.

Robertson, A. H. F., Dixon, J. E., Brown, S., Collins, A., Morris, A., Pickett, E., Sharp, I., Ustaömer, T. 1996. Alternative tectonicmodels for the Late Palaeozoic–Early Tertiary development of Tethys in the Eastern Mediterranean region. Geological Society, London, Special Publications: 105, 239–263.

Robertson, A. H. F., Parlak, O., Ustaomer, T. 2012. Overview of the Palaeozoic neogene evolution of neotethys in the Eastern Mediterranean region (Southern Turkey, Cyprus, Syria). Petroleum Geoscience: 18, 381–404.

Robertson, A. H. F., Parlak, O., Rızaoğlu, T., Ünlügenç, U. C., Inan, N., Taslı, K., Ustaömer, T. 2007. Tectonic evolution of the South Tethyan ocean: evidence from the Eastern Taurus mountains (Elazığ region, SE Turkey), in Deformation of the Continental Crust: The Legacy of Mike Coward, Eds. Ries, A. C., Butler, R. W. H., Graham, R. H., Geological Society of London, Special Publications: 272, 233–272.

Seghedi, I., Downes, H. 2011. Geochemistry and tectonic development of Cenozoic magmatismin the Carpathian–Pannonian region. Gondwana Research: 20, 655–672.

Sun, S. S., McDonough, W. F. 1989. Chemical and isotopic systematics of oceanic basalts: implications for mantle composition and processes, n Magmatism in the Ocean Basins. Eds. Saunders, A. D., and Norry, M. J., Geological Society of London, Special Publications: 42, 313–347.

Sungurlu, O. 1974. VI. Bölge kuzey sahalarının jeolojisi. Türkiye İkinci Petrol Kongresi Bildirileri. Ankara, 85–107.

Sungurlu, O., Perinçek, D., Kurt, G., Tuna, E., Dülger, S., Çelikdemir, E., Naz, H. 1985. Elazığ–Hazar–Palu Alanının Jeolojisi. Türkiye Petrolleri Anonim Ortaklığı: 29, 83–190.

Şaşmaz, A., Türkyilmaz, B., Öztürk, N., Yavuz, F., Kumral, M. 2014. Geology and geochemistry of Middle Eocene Maden complex ferromanganese deposits from the Elazığ–Malatya region, eastern Turkey. Ore Geology Reviews: 56, 352–372.

Şengör, A. M. C., Özeren, M. S., Keskin, M., Sakınç, M., Özbakır, A. D., Kayan, I. 2008, Eastern Turkish high plateau as a small Turkic–type orogen: implications for post–collisional crust–forming processes in Turkic–type orogens. Earth Science Reviews: 90, 1–48.

Şengör, A. M. C., Yılmaz, Y. 1981. Tethyan evolution of Turkey: a plate tectonic approach. Tectonophysics: 75, 181–241.

Tatsumi, Y. 1989. Migration of fluid phases and genesis of basalt magmas in subduction zones. Journal of Geophysical Research: 94, 4697–4707.

Tekin, U. K., Ural, M., Goncüoglu, M. C., Arslan, M., Kürüm, S. 2015. Upper Cretaceous Radiolarian ages from an arc–backarc within the Yüksekova Complex in the Southern Neotethyan melange, SE Turkey. Comptes Rendus Palevol: 14, 73–84.

Ural, M., Arslan, M., Goncüoglu, M. C. Tekin, U. K., Kürüm, S. 2015. Late Cretaceous arc and back–arc formation within the southern Neotethys: whole–rock, trace element and Sr–Nd Pb isotopic data from basaltic rocks of the Yüksekova Complex (Malatya–Elazig, SE Turkey). Ofioliti: 40, 52–72.

Ustaömer, P. A., Ustaömer, T., Collins, A. S., Robertson, A. H. F. 2009. Cadomian (Ediacaran–Cambrian) arc magmatism in the Bitlis Massif, SE Turkey: magmatism along the developing northern margin of Gondwana. Tectonophysics: 473, 99–112.

Ustaömer, P. A., Ustaömer, T., Gerdes, A., Robertson, A. H. F., Collins, A. S. 2012. Evidence of Precambrian sedimentation/magmatism and Cambrian metamorphism in the Bitlis Massif, SE Turkey utilising whole–rock geochemistry and U–Pb LA–ICP–MS zircon dating. Gondwana Research: 21, 1001–1018.

Uzunçimen, S., Tekin, U. K., Bedi, Y., Perinçek, D., Varol, E., Soycan, H. 2011. Discovery of the Late Triassic (Middle Carnian–Rhaetian) radiolarians in the volcano–sedimentary sequences of the Kocali Complex, SE Turkey: Correlation with the other Tauride units. Journal of Asian Earth Sciences: 40, 180–200.

Varol, E., Bedi, Y., Tekin, U.K., Uzuncimen, S. 2011. Geochemical and petrological characteristics of late Triassic basic volcanic rocks from the Kocali complex, SE Turkey: implications for the Triassic evolution of southern Tethys. Ofioliti: 36, 101e115.

Verdel, C., Wernicke, B. P., Hassanzadeh, J., Guest, B. 2011. A Paleogene extensional arc flare–up in Iran. Tectonics: 30. http://dx.doi.org/10.1029/2010TC002809 TC3008.

Vidal, Ph., Cocherie, A., Le Fort, P. 1982. Geochemical investigations of the origin of the Manaslu leucogranite (Himalaya, Nepal) Geochimica et Cosmochimica Acta: 46, 2279–2292.

Yazgan, E. 1981. Doğu Toros'larda Etkin Bir Paleo Kıta Kenarı Etüdü (Üst Kretase– Orta Eosen), Malatya–Elazığ, Doğu Anadolu. Yerbilimleri: 7, 83–104.

Yazgan, E. 1983. A geotraverse Between the Arabian Platform and the Munzur Nappes. Geology of the Taurus Belt. Int. Symp. Guide Book for Excursion V., 17, MTA Ankara.

Yazgan, E. 1984. Geodynamic Evolution of the Eastern Taurus Region (Malatya–Elazığ area, Turkey). in International Symposium on the Geology of the Taurus Belt, Eds. Tekeli, O., and Göncüoğlu, M. C., Proceedings, 26–29 September, MTA, Ankara, 199–208.

Yazgan, E., Chessex, R. 1991. Geology and tectonic evolution of the Southeastern Taurides in the region of Malatya. Turkish Association of Petroleum Geology Bulletin 3, 11–42.

Yazgan, E., Michard, A., Whitechurch, H., Montigny, R. 1983. Le taurus de Malatya (Turquie orientale) element de la suture sud–tethysienne. Bulletin de la Société géologique de France: 25, 59–69.

Yıldırım, E. 2010. Çelikhan–Sincik (Adıyaman) arasındaki magmatik kayaçların petrolojisi. Firat University, Institute of Science and Technology, PhD. Thesis, Elazığ–Turkey, 247 p.

Yılmaz, Y. 1993. New evidence and model evolution of the southeast anatolian orogen. Geological Society of America Bulletin: 105, 251–271.

Yılmaz, Y., Yigitbaş, E. 1991. The Different ophiolitic–metamorphic assemblages of the SE Anatolia and their significance in the geological evolution of the region. In: Proc 8th Petrol. Congr. Turkey (in Turkish with English abstract), pp. 18–140.

Yılmaz, Y., Yiğitbaş, E., Genç, Ş. C. 1993. Ophiolitic and Metamorphic Assemblages of Southeast Anatolia and Their Significance in the Geological Evolution of the Orogenic Belt. Tectonics: 12, 1280–1297.

Yılmaz, Y., Yiğitbaş, E., Yıldırım, M. 1987. Güneydoğu Anadolu’da Triyas sonu tektonizması ve bunun jeolojik anlamı. Türkiye 7. Petrol Kongresi Bildiriler: 65–77.

Yiğitbaş¸ E., Genç, S.C., Yılmaz, Y., 1993. Güneydoğu Anadolu Orojenik kuşağında Maden Grubu’nun tektonik konumu ve jeolojik önemi. A.Suat Erk Jeoloji Sempozyumu, 2–5 Eylül, Ankara Üniv, Fen Fakültesi, Ankara, 251–264.

Yiğitbaş, E., Yılmaz, Y. 1996. New evidence and solution to the Maden complex controversy of the Southeast Anatolian orogenic belt (Turkey). Geologische Rundschau: 85, 250–263.

Zou, H. B., Zindler, A., Xu, X. S., Qi, Q. 2000. Major, trace element and Nd–Sr and Pb isotope studies of Cenozoic basalts in SE China Mantle sources, regional variations and tectonic significance. Chemical Geology: 171, 33–47.